

Coherent all-optical switching by resonant quantum-dot distributions in photonic band-gap waveguides

Dragan Vujic* and Sajeev John

Department of Physics, University of Toronto, 60 St. George Street, Toronto, Ontario, Canada M5S-1A7

(Received 10 October 2007; published 17 December 2007)

We study the detailed propagative characteristics of optical pulses in photonic band-gap (PBG) waveguides, coupled near resonantly to inhomogeneously broadened distributions of quantum dots. The line centers of the quantum-dot (QD) distributions are placed near a sharp discontinuity in the local electromagnetic density of states. Using finite-difference time-domain (FDTD) simulations of optical pulse dynamics and independent QD susceptibilities associated with resonance fluorescence, we demonstrate subpicosecond switching from pulse absorption to pulse amplification using steady-state optical holding and gate fields with power levels on the order of 1 milliwatt. In the case of collective response of QDs within the periodic dielectric microstructure, the gate power level is reduced to 200 microwatt for room temperature operation. In principle, this enables 200 Gbits per second optical information processing at wavelengths near 1.5 microns in various wavelength channels. The allowed pulse bandwidth in a given waveguide channel exceeds 0.5 THz allowing switching of subpicosecond laser pulses without pulse distortion. The switching contrast from absorption to gain is governed by the QD oscillator strength and dipole dephasing time scale. We consider dephasing time scales ranging from nanoseconds (low-temperature operation) to one picosecond (room-temperature operation). This all-optical transistor action is based on simple Markovian models of single-dot and collective-dot inversion and switching by coherent resonant pumping near the photon density of states discontinuity. The structured electromagnetic vacuum is provided by two-mode waveguide architectures in which one waveguide mode has a cutoff that occurs, with very large Purcell factor, near the QDs resonance, while the other waveguide mode exhibits nearly linear dispersion for fast optical propagation and modulation. Unlike optical switching based on Kerr nonlinearities in an optical cavity resonator, switching power levels and switching speeds for our QD device are not inversely proportional to cavity quality factors.

DOI: [10.1103/PhysRevA.76.063814](https://doi.org/10.1103/PhysRevA.76.063814)

PACS number(s): 42.65.Wi, 42.65.Pc, 42.50.Gy, 42.79.-e

I. INTRODUCTION

Photonic band-gap (PBG) materials [1,2] are a special class of three-dimensional (3D) periodic dielectric structures that, through multiple light scattering and interference, enable the fundamental phenomenon of light localization [3]. Light localization provides a foundation for broadband integrated optics within 3D optical circuit architectures [4,5]. Unlike semiconductor-based electronic microchips that support a single channel of information through electrical current, an optical microchip based on photonic band-gap materials can support many parallel streams of optical information through different wavelength channels passing through a single waveguide. As an optical analog of semiconductors, photonic crystals (PC's) offer an opportunity to create the all-optical analogs of diodes, transistors, and switches [6–8].

Simple optical switching devices, considered previously, consist of one Kerr nonlinear defect cavity near or inside a photonic crystal waveguide [9–15]. Such architectures enable switching of light with light through nonlinear change of the resonant frequency of the cavity. In an earlier paper [16], we delineated the inverse relation between switching power requirements and switching time scales for Kerr nonlinear cavity resonators. High quality-factor optical resonators also lead to distortion of short pulses, leading to fundamental limitations on the functionality of this switching

mechanism. In this paper, we demonstrate by direct numerical simulation of optical pulses in PBG waveguides, seeded with an inhomogeneously broadened collection of nearly resonant quantum dots, that distortionless all-optical switching on the subpicosecond scale is in principle possible. In this bimodal PBG waveguide, one of the modes has a sharp cutoff near the center of the inhomogeneously broadened quantum-dots distribution, enabling single quantum-dot population inversion and switching by a coherent cw laser field [17–19]. The optical cw power level required for switching of the signal pulse from absorption to amplification depends primarily on the breadth of the quantum dot (QD) inhomogeneous line broadening, the uniformity and overlap of the waveguide mode with QDs, and the magnitude of the electromagnetic density of states discontinuity (as determined by the length of the waveguide channel). Unlike Kerr nonlinear switching, a prohibitively high switching power level is not required to achieve subpicosecond switching times [9–16]. Instead, the resonant QD switching device exhibits an indirect relationship between switching power level and switching time scales, mediated by the width of the QD distribution. A broader QD distribution provides larger bandwidth for amplification (faster switching) but requires larger driving fields to invert the majority of QDs. Typical cw power levels in our simulations range from a few hundred μW to a few mW.

Within the narrow, subwavelength, confines of our photonic crystal waveguides, these power levels translate into peak field strengths, A^{cw} , of 5.7×10^4 V/cm to 1.6×10^5 V/cm. Electric fields within rods containing QDs, ranging from

*dvujic@physics.utoronto.ca

4.0×10^4 V/cm to 10^5 V/cm, provide Rabi frequencies, $\hbar\epsilon = \mu \cdot \mathbf{A}^{\text{cw}}$, in the range of 2.7 meV to 6.8 meV, if the quantum-dot dipole transition matrix element is chosen to be $\mu = 1.09 \times 10^{-28}$ C m. By comparison, the QD transition frequency $\hbar\omega_A \approx 0.8$ eV for resonant coupling to light at 1.5 micron wavelength. This strong coupling between the QD dipole and the cw driving field leads to Mollow splitting [19,20] of the QD excited state, where the separation between the upper and lower Mollow sideband is in the range from 2% to 5% of the bare transition frequency of ω_A . In our model the typical separation, R , between the centers of QDs is 30 nm. This limits the energy scale for resonance dipole-dipole interactions to roughly $\frac{\mu^2}{4\pi\epsilon_0 R^3} \approx 25$ μeV [21]. This is small compared to the Rabi energy scale, $\hbar\epsilon$. Consequently, the QD dipoles respond dominantly to the external field rather than neighboring QDs. This is particularly important for the case of collective QD switching [6]. When these separate Mollow sidebands experience a large (roughly a factor of 100) difference in the local electromagnetic density of states (LDOS), provided by the “colored vacuum” of the PBG material, the QD may undergo switching [6,8,17–19] by a small change in the amplitude of the coherent resonant pumping field. Very large Purcell factors [22] in the high LDOS spectral range ensure strong radiative coupling, which dominates over phonon-mediated dephasing and other relaxation effects. Provided that the Mollow sideband separation is not smeared out by inhomogeneous QD line broadening, the PBG waveguide, suitably seeded with QDs, will act as a switching device for certain signal pulses passing through the waveguide.

Optical switching based on quantum dots in a photonic crystal is a subject of recent experimental interest. For example, one switching device in a photonic crystal waveguide seeded with quantum dots with switching time of 15 ps and peak power of around 50 mW has recently been reported [10]. However this device does not make use of coherent resonant switching as considered in our paper. Instead it relies on the nonresonant Kerr nonlinearity provided by QDs. This is among the fastest all-optical switching results in PC's, experimentally reported. Given the low group velocities in this experimental PC waveguide, a significant amount of time is required for light to traverse the long (around 600 μm) waveguide device. For an optical group velocity of 0.25 of the speed of light in vacuum, an additional 8 ps must be imputed to the true switching time of this device. Other similar examples reveal that state-of-the-art all-optical switching is not yet competitive with on-chip electronic transistors in information processing. An important benchmark for photonics is to achieve on-chip all-optical switching devices operating at powers below 1 milliwatt, that can switch subpicosecond laser pulses with subpicosecond switching time.

Recently, a few theoretical papers [6–8,17,19] have explored a new mechanism for “controlling light with light,” by engineering the electromagnetic vacuum density of states in a three-dimensional PBG microchip seeded with quantum dots. In the present paper, we simulate the switching of subpicosecond optical pulses in a simplified two-dimensional (2D) photonic crystal system where the QDs response to an

electromagnetic density of states discontinuity is introduced as an ansatz. This model system is designed to simulate the behavior of an actual device embedded in a 2D-3D PBG heterostructure [8,23], where the density of states feature appears naturally. We investigate, numerically, all-optical transistor action in photonic crystal waveguide seeded with QDs with parameters chosen to mimic InGaAs/GaAs or InAs/InGaAs quantum dots. We utilize two simple designs for bimodal PC waveguides with one propagating mode allowing fast light propagation, while the second mode exhibits a cutoff frequency with vanishing group velocity somewhere inside the band gap. Both designs provide a very large and sudden change of the local electromagnetic density of states at the cutoff frequency. The magnitude of the density of states jump increases with the length of the waveguide channel contained in the switching device [8]. Our numerical simulations for the 2D system (with no propagation allowed normal to the 2D plane) simulate the behavior of a more realistic 2D-3D PBG heterostructure [23] in which one thin 2D layer with defect line (waveguide) is embedded in a 3D PBG material. We find that it is possible to design and simulate an all-optical transistor operating with 1 ps laser pulses with switching time of 1 ps. Even with relatively weak evanescent coupling of optical fields to QDs, our optical transistor requires the change of the driving field power (gate field) of only a few hundred microwatt, to switch the device from the absorbing to amplifying state or vice versa. The combination of high-speed switching, low-power thresholds, and multichannel (multiwavelength) operation, all on-chip, suggest an interesting alternative to electronic information processing.

Section II of the paper discusses the relative merits of various PC structures exhibiting electromagnetic density of state jumps inside the waveguide. Section III introduces basic equations for wave propagation in the waveguide, defines the response of QDs to electromagnetic fields, and describes optical and material parameters for the QDs in our simulation. Section IV describes our numerical method and presents simulation results. Section V discusses how our present results based on single QD optical switching might be improved if significant groups of QDs (all experiencing the same optical field) undergo coherent, collective switching. Section VI summarizes our results and suggests mechanisms for lowering the optical switching power threshold and improving the switching contrast without sacrificing switching speed.

II. WAVEGUIDE ARCHITECTURES FOR QD SWITCHING

As an example of an all-optical QD switching architecture, we choose an idealized 2D structure consisting of a square lattice (lattice constant a) of dielectric rods made of GaAs ($\epsilon_r=9$) with radius $r=0.3a$, embedded in air. This structure has band gap for the transverse magnetic (TM) polarized light between $\omega_{\min}=0.265(2\pi c/a)$ and $\omega_{\max}=0.335(2\pi c/a)$, where c is the speed of light in vacuum. In this idealized 2D system, light propagation is not allowed in the vertical direction perpendicular to the 2D plane. In a real 3D system, the vertical confinement may be achieved by 3D

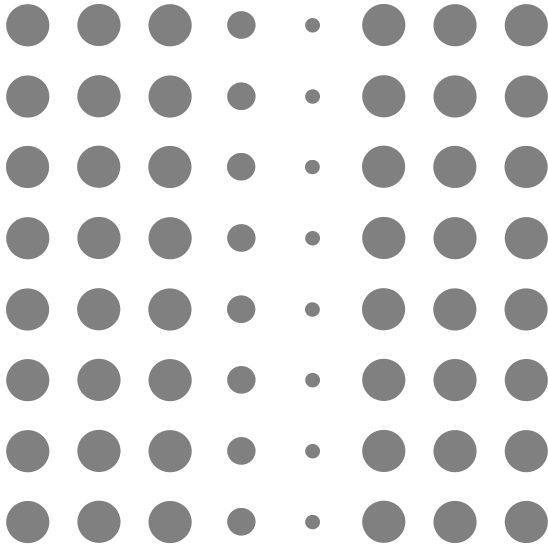


FIG. 1. Generic layer structure exhibiting a discontinuous electromagnetic density of states within the gap of 2D-3D PBG heterostructure.

PBG cladding material above and below this 2D microchip layer [24].

Unlike an earlier study [8] of electromagnetic density of states engineering in a 3D PBG material, we consider an inhomogeneous distribution of quantum dots within the waveguide pillars and we use specific values of the QD dipole transition matrix elements obtained from experiments on InGaAs dots in GaAs and InAs dots in InGaAs. In order to achieve high-speed (picosecond scale) switching, the Mollow splitting [17–19] of the QDs must be large compared to the optical bandwidth of the signal pulse to ensure that all Fourier components of the pulse interact with single Mollow sideband. For picosecond scale switching, this requires a Rabi frequency of the cw driving field to be on the order of THz.

In order to achieve QD switching by resonance fluorescence in a photonic band-gap waveguide, our waveguide architecture must provide a large jump (typically a factor of 100 over a frequency interval of $10^{-4}\omega_A$, where ω_A is the QD transition frequency) of the electromagnetic density of states inside the gap [19] (see Fig. 7). One possible architecture consists of changing the radius of the dielectric rods in two adjacent lines as shown in Fig. 1. More specifically the waveguide is made by reducing the rod radius in one line to $r_1=0.1a$, and in the next line to $r_2=0.2a$. Dispersion lines calculated at resolution of 20 pixels per lattice constant, using finite-difference time-domain (FDTD) [25,26] method are shown in Fig. 2. Mode 1 has group velocity $0.23c$ at the frequency for which mode 2 has cutoff [$\omega_{\text{cutoff}}=0.2966(2\pi c/a)$]. Maximal illumination of the cutoff mode is on the rods with $r=0.2a$. Accordingly, the quantum dots are embedded in these rods. Mode 1 propagates predominantly through the defect line made by reducing rods to $r=0.1a$, but there is significant overlap with rods where quantum dots are located. This provides interaction of the propagating mode with nonlinear dielectric rods to enable switching.

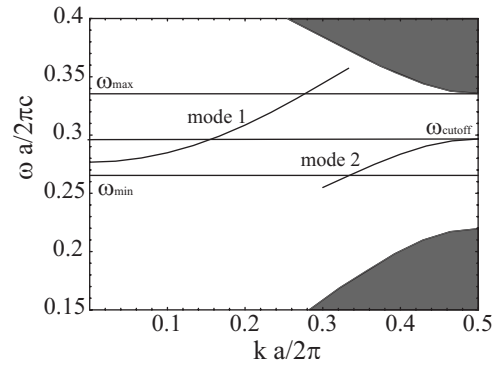


FIG. 2. Dispersion lines of the waveguide shown on the Fig. 1. Mode 2 provides large jump of the local density of states around cutoff frequency, while mode 1 allows fast light propagation in the vicinity of the cutoff frequency of mode 2.

In general a variety of different architectures provide a structured electromagnetic vacuum for coherent optical switching of QDs. For practical purposes, the ideal architecture should also provide (i) the placement of a large number of QDs into the relevant dielectric pillars, (ii) strong coupling between the relevant optical modes and the active region of the waveguide, and (iii) a relatively uniform intensity of the driving field over the active region so that the maximum number of QDs undergo switching simultaneously. These criteria enable lower power thresholds for all-optical switching. In order to illustrate these points, we compare and contrast two specific waveguide architectures below.

Our numerical investigations reveal that we can introduce two adjacent lines of defects to support the cutoff mode, both with $r_2=0.2a$, without incurring significant change of dispersion properties of the waveguide. By using both defect lines to host the cutoff mode, we can embed a larger number of quantum dots in the waveguide and thereby increase the non-linear response. Moreover, we find that bringing these two defect lines closer to each other, and making them slightly elliptical, we can further increase the volume of the rods containing quantum dots. We refer to the design shown in Fig. 3 as Architecture 1 for our simulations of optical switching with resonant quantum dots. Our overall waveguide architecture consists of changing the rods in three lines in the middle of the 2D PC layer. In the first defect line, the rod radius is reduced to $r_1=0.15a$ and these rods are shifted by $a/4$ toward the center of the waveguide. In the remaining two defect lines, elliptical rods are introduced with semimajor and semiminor axes of $0.3a$ and $0.25a$, respectively. The centers of these elliptical defect lines are moved closer to each other (the left line is moved right by $a/10$ and the right line is moved left by $3a/20$). The remainder of the photonic crystal is unmodified.

Dispersion lines of this bimodal waveguide, calculated by FDTD method with resolution of 20 points per lattice constant, are shown in Fig. 4. The propagation mode (nearly linear dispersion) has group velocity $v_g \approx 0.2c$ for the frequency at which mode 2 has its cutoff [$\omega_{\text{cutoff}}=0.27655(2\pi c/a)$]. The maximal illumination of mode 2 is on the elliptical rods, where the quantum dots are located. In order to achieve optimal illumination of quantum dots, we

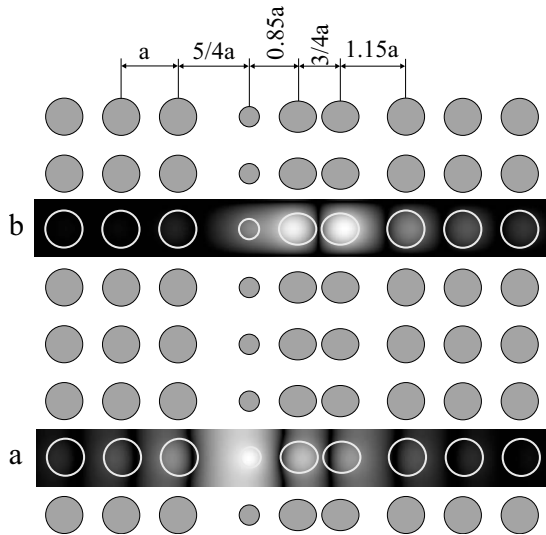


FIG. 3. Architecture 1 consists of a 2D layer (embedded within a 3D heterostructure), made of dielectric rods ($n=3$) with radius $0.3a$. A bimodal waveguide is made by reducing rods in one line to $0.15a$, and including elliptical rods with semimajor and semiminor axis of $0.3a$ and $0.25a$, respectively. All defect lines are moved closer to each other. (a) Steady-state illumination of propagation mode oscillating near cutoff frequency $0.27655(2\pi c/a)$. (b) Steady-state illumination of cutoff mode oscillating at cutoff frequency.

embed them only in the one line of elliptical rods close to the propagating line. Mode 1 propagates predominantly through the defect line consisting of small rods with radius $r_1 = 0.15a$. As in the illustration of Fig. 1, Architecture 1 provides only evanescent overlap of the propagating signal beam with the quantum dots.

In the ideal operation of this switching device, it is advantageous to illuminate mode 2 by an internal cw light source or to electrically pump the QDs and bring them to just below their switching threshold by a holding field. Mode 2 has vanishing group velocity and, as such, it cannot be modulated rapidly. The “gate field,” on the other hand, performs the switching operation and should propagate through mode 1 if rapid modulation is required. This type of bimodal op-

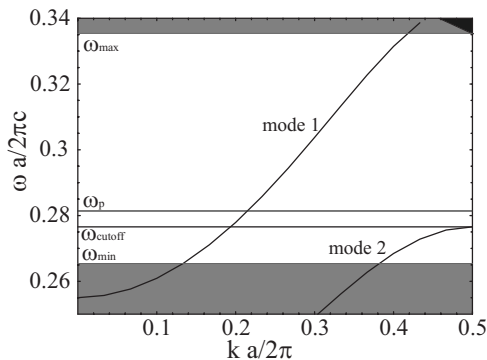


FIG. 4. Dispersion lines of the waveguide shown on the Fig. 3. (a) Propagating mode (mode 1) conveys ultrafast optical pulse and (b) cutoff mode (mode 2) provides the required large jump of the local density of states around cutoff frequency.

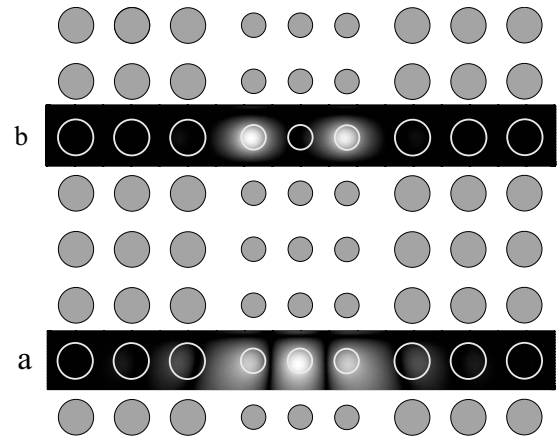


FIG. 5. Architecture 2 consists of a 2D layer (embedded within a 3D heterostructure), made of dielectric rods ($n=3$) with radius $0.3a$. A bimodal waveguide is made by reducing rods in three lines to $0.2a$ and by shifting the two outer lines of reduced rods toward the middle by $a/6$. (a) Steady-state intensity distribution of propagating mode (mode 1, see Fig. 6) in the vicinity of cutoff frequency of mode 2 and (b) steady-state intensity distribution of cutoff mode (mode 2).

eration, however, leads to optical interference between the holding and gate fields leading to large intensity variations between equivalent points within the waveguide. Moreover, the nonlinear response slightly changes the dispersion relations of the guided modes. This can lead to temporal intensity oscillations at frequencies close to the cutoff frequency, that are sensitive to nonlinear coupling. For the sake of numerical stability it is convenient to control the coherent state of quantum dots with a single high-intensity laser field (acting as both holding and gate fields) oscillating at a single frequency propagating through mode 1. In this case, the time-averaged cw illumination of the nonlinear rods is stationary in time and uniform throughout the waveguide (see Fig. 8). There are two drawbacks to conveying both the holding and gate fields through mode 1. This leads to higher overall power requirements because the optical fields are evanescently coupled to the active region of the waveguide. In addition, the illumination pattern, from mode 1, is less uniform over the QD distribution. This nonuniformity effectively broadens the intrinsic inhomogeneous distribution of the QDs arising from their size distribution. There is more cancellation of QDs above inversion threshold (in strong field regions) with QDs below threshold (in weak field regions). Despite these drawbacks, we are able to demonstrate stable switching characteristics of the overall device at power levels less than 1 mW.

In order to effect stronger coupling between the holding, gate, and signal fields we consider a second waveguide architecture for all-optical switching depicted in Fig. 5. We refer to this design as Architecture 2. This consists of replacing three lines of rods with smaller rods in the middle of the waveguide. The smaller rods each have radius $r_1 = 0.2a$. The two outer lines of reduced rods are shifted toward the middle by $a/6$, in order to increase the group velocity of the signal. In Architecture 2, mode 2 (see, band structure, Fig. 6) has cutoff at $\omega_{\text{cutoff}} = 0.2969(2\pi c/a)$, once again providing large

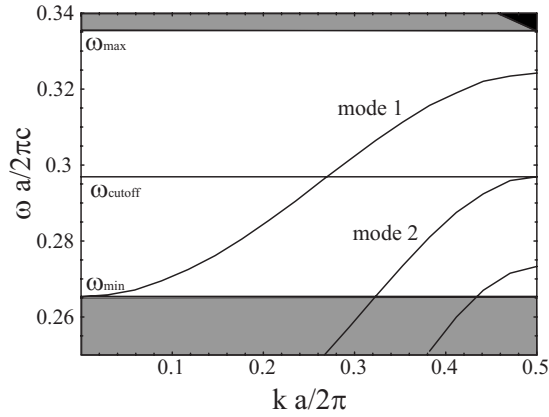


FIG. 6. Dispersion lines of the waveguide (Architecture 2) shown in Fig. 5. Propagating mode (mode 1) allows ultrafast pulse propagation, while cutoff mode (mode 2) provides large jump of LDOS around cutoff frequency $\omega_{\text{cutoff}}=0.2969(2\pi c/a)$.

jump of the local density of states. Mode 2 is antisymmetric with respect to the waveguide center and has highest illumination on the two outer columns of small rods where the quantum dots are embedded. In contrast, mode 1 is symmetric about the waveguide center and has highest illumination on the central rods. Nevertheless, mode 1 has strong overlap with QD regions located in both outer lines of small dielectric rods. This propagating mode exhibits nearly linear dispersion with group velocity of $v_g=0.18c$ for the frequencies in the vicinity of the cutoff frequency of mode 2.

In order to make our simulations more realistic, we seed the quantum dots with different transition frequencies at each different mesh point in the nonlinear rods. The transition frequency, ω_{A_j} , of the j th quantum dot is normally distributed around the central frequency ω_A . A Gaussian distribution of transition frequencies with a small width enables an improved operating bandwidth of the switching device. This is necessary for switching of short (~ 1 ps) pulses. This inhomogeneous broadening also reduces the spatially averaged real part of linear susceptibility, thereby reducing pulse reflection at the entry port of the nonlinear waveguide. In the absence of this broadening, the QDs present a large impedance mismatch for a pulse entering the device from a passive waveguide. Such a mismatch would lead to unwanted pulse reflection. Our numerical simulations reveal that a transition frequency distribution with relative full-width at half-maximum (FWHM) $\frac{\Delta\omega_A}{\omega_A} \approx 0.4\%$ is ideal for constructing a good all-optical transistor. A quantum-dot distribution with larger FWHM provides a smaller nonlinear effect and requires higher gate and holding field powers, but enables faster switching. In general, detuning between cw laser (holding plus gate) field and central atomic transition frequency also places an upper bound on the QD transition frequency distribution. For atomic switching to occur on a given Mollow sideband for a given photon density of states jump, it is necessary for the atomic transition frequency to lie on a specific side of the driving field frequency [6]. Larger detuning between cw laser field and central transition frequency of quantum dots accommodates a large inhomogeneous distribution but leads to higher switching threshold.

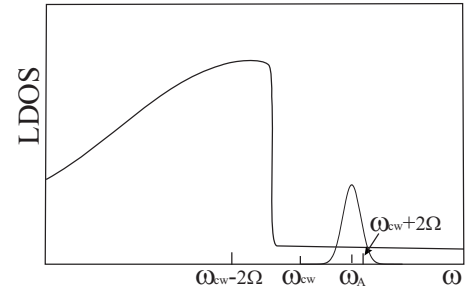


FIG. 7. A schematic representation of the local density of states generated inside the bimodal photonic crystal waveguides and the relevant frequencies for resonance fluorescence. Atomic transition frequencies, ω_{A_j} , are normally distributed around central atomic transition frequency ω_A . With a strong cw laser field at frequency ω_{cw} , the Mollow fluorescence sidebands are centered at $\omega_{\text{cw}} \pm 2\Omega$, where Ω is the Rabi frequency.

On the other hand, a very narrow distribution of quantum-dot frequencies is difficult to achieve from a materials synthesis point of view. State-of-the-art techniques for precision placement of QDs with very narrow size distribution enable $\frac{\Delta\omega_A}{\omega_A} \approx 1.0\%$ [27–30]. Accordingly, we consider all-optical transistor action with this amount of line broadening as well.

III. COUPLED EQUATIONS FOR OPTICAL PROPAGATION AND QUANTUM-DOT RESPONSE

Near the cutoff frequency of mode 2 (Fig. 4) in Architecture 1 (Fig. 3), a sharp jump in the local photon density of states occurs at the QD positions (see Fig. 7). This facilitates coherent optical switching by resonance fluorescence. The spectral properties of two level atoms driven by an external laser field in such a “colored” electromagnetic vacuum have been theoretically analyzed earlier [19], without consideration of their influence on optical wave propagation. It was shown that the absorption spectrum of a signal field (laser pulse) on a specific Mollow sideband can be switched to a gain spectrum by small variation of the cw driving field. This variation of the driving field performs the operation of a gate in this “photonic transistor.” In this section, we consider the detailed dynamical interplay between optical waves and an inhomogeneous distribution of QDs in the bimodal PBG waveguide.

Ideally, coherent control of the quantum dots takes place through two separate cw optical fields. A holding field, oscillating on cutoff frequency, can be realized by an external cw laser field or internal coherent sources located within the waveguide itself. The intensity of this holding field should be sufficiently large to drive the majority of QDs to just below their switching threshold. However, the holding field should remain sufficiently low that the system is not pushed into the switching critical regime, characterized by fluctuations and noise [6]. The gate field is provided by one external cw laser field oscillating near the cutoff frequency and preferably at slightly higher frequency in the single-mode spectral region of the bimodal waveguide. Operation of the gate field in the single-mode region, just above the density of states jump in

Fig. 4, reduces the possibility of instabilities arising from nonlinear coupling between mode 1 and mode 2. Turning the gate field on and off switches the device back and forth from below threshold, through the critical regime characterized by fluctuations, to above threshold where it can then amplify a (third) signal beam. The coherent state of our two-level atoms is controlled by the superposition of the holding and gate fields. We call this the “driving field.” The detailed dynamical response of two-level systems, near a density of states jump, and driven by laser fields at two separate frequencies leads to a more complex Mollow sideband structure [31]. In order to simplify our investigation and to avoid interference between two separate fields, we combine the holding and gate fields into a single laser field operating in mode 1 just above the cutoff of mode 2 (Fig. 4). In what follows, we refer to this single driving field as the “cw laser field” or the “control beam.” While this reduces the complexity of our numerical simulations, this choice of control field leads to evanescent (weaker) coupling to the QDs and results in less uniformity of illumination of the QDs. This variation of the control field intensity from one QD to another is a major source of inhomogeneous broadening, over and above the actual size distribution of QDs. Nevertheless, this choice of control beam allows us to establish “proof of principle” for the operation of our optical transistor, albeit at an artificially elevated threshold intensity for switching.

It is well known that a single strong monochromatic laser field oscillating on (or near) resonance to an atomic transition gives rise to the triplet resonance fluorescence Mollow spectrum [20]. The Mollow spectrum in PBG waveguides has also been studied in detail [19]. Here we provide a brief review of the mechanism of the population inversion of two-level atoms characterized by ground states $|1\rangle_j$ and excited states $|2\rangle_j$ in an engineered vacuum. Index j refers to the j th atom. The Hamiltonian of the system in the interaction picture has the form $H=H_0+H_{AF}+H_{AL}$. Here, $H_0=\hbar\sum_j\Delta_{A,j}L\sigma_{3,j}+\sum_\lambda\hbar\Delta_\lambda a_\lambda^\dagger a_\lambda$ is the noninteracting Hamiltonian of the bare atomic and the photonic reservoir, with $\Delta_{A,j}=\omega_{A,j}-\omega_{cw}$ and $\Delta_\lambda=\omega_\lambda-\omega_{cw}$. $\omega_{A,j}$ is the atomic transition frequency of the j th quantum dot, ω_{cw} is the frequency of the cw laser field (driving field), and ω_λ is the frequency of a photon in mode λ in the electromagnetic reservoir. The interaction between the atoms and photonic reservoir is given by $H_{AF}=-\hbar\sum_{\lambda,j}g_{\lambda,j}(a_\lambda^\dagger\sigma_{-,j}-\sigma_{+,j}a_\lambda)$ and the interaction between the atomic system and laser field is given by $H_{AL}=\sum_j\hbar\epsilon_j(\sigma_{-,j}-\sigma_{+,j})$. Here, $\sigma_{-,j}$ and $\sigma_{+,j}$ are the atomic excitation and deexcitation operators, $\sigma_{3,j}$ is the atomic inversion operator, and $g_{\lambda,j}$ is the coupling constant between the j th atom and the reservoir mode λ . Finally, a_λ and a_λ^\dagger are the photon annihilation and creation operators and $\epsilon_j=\mu\cdot\mathbf{A}_j^{cw}/\hbar$ is the resonance Rabi frequency of the atom with the dipole transition matrix element μ and applied laser field amplitude \mathbf{A}_j^{cw} . The Hamiltonian can be solved in the dressed atom basis defined by $|\tilde{1}\rangle_j=\mathbf{c}_j|1\rangle_j+\mathbf{s}_j|2\rangle_j$ and $|\tilde{2}\rangle_j=-\mathbf{s}_j|1\rangle_j+\mathbf{c}_j|2\rangle_j$, where $\mathbf{s}_j^2=\frac{1}{2}(1-\frac{\Delta_{A,j}}{\Omega_j})$ and $\mathbf{c}_j^2=\frac{1}{2}(1+\frac{\Delta_{A,j}}{\Omega_j})$. The generalized Rabi frequency of j th QD is defined as $\Omega_j=[(\frac{\mu\mathbf{A}_j^{cw}}{\hbar})^2+\frac{\Delta_{A,j}^2}{4}]^{1/2}$.

In the dressed basis, the total Hamiltonian becomes $H=H_0+H_I$, with $H_0=\sum_\lambda\hbar\Delta_\lambda a_\lambda^\dagger a_\lambda+\hbar\sum_j\Omega_j R_{3,j}$ and H_I

$=i\hbar\sum_{\lambda,j}g_{\lambda,j}[a_\lambda^\dagger(\mathbf{c}_j\mathbf{s}_j R_{3,j}+\mathbf{c}_j^2 R_{12,j}-\mathbf{s}_j^2 R_{21,j})]+H.c.$ Here, $R_{12,j}$ and $R_{21,j}$ are dressed atomic excitation and deexcitation operators, while $R_{3,j}$ is the dressed atom inversion operator. In the time-dependent interaction picture generated by the unitary operator $U=\exp(-iH_0t)$, the interaction Hamiltonian becomes

$$\begin{aligned}\tilde{H}_I(t) &= i\hbar\sum_{\lambda,j}g_{\lambda,j}\{a_\lambda^\dagger[\mathbf{c}_j\mathbf{s}_j R_{3,j}\exp(i\Delta_\lambda t)+\mathbf{c}_j^2 R_{12,j}] \\ &\quad \times \exp[i(\Delta_\lambda-2\Omega_j)t]-\mathbf{s}_j^2 R_{21,j} \\ &\quad \times \exp[i(\Delta_\lambda+2\Omega_j)t]\}+H.c.,\end{aligned}$$

and the time-dependent dressed atomic operators are $\tilde{R}_{-,j}(t)=R_{12,j}(0)\exp(-2i\Omega_j t)$, $\tilde{R}_{+,j}(t)=R_{21,j}(0)\exp(2i\Omega_j t)$, and $\tilde{R}_{3,j}(t)=R_{3,j}(0)\exp(2i\Omega_j t)$.

There are three separate models for atom-field interactions relevant to the optical switching problem. In model I, the QDs are considered to be independent of each other and respond individually to the applied field [19]. Furthermore, the Mollow sidebands at frequencies at ω_{cw} and $\omega_{cw}\pm 2\Omega_j$ are assumed to occur in spectral regions where the photon density of states is smooth (leading to Markovian response) even though there may be a sharp density of states discontinuity nearby. This independent atom switching with Markovian dynamics has been studied in detail before [17,19]. In model II, a large group of atoms, experiencing the same electromagnetic field, exhibits collective switching [6]. In this case the overall magnitude of medium response near threshold is much larger and much sharper (larger switching contrast) than for independent atoms. In model III, the detailed non-Markovian dynamics of an atom near an abrupt jump in the photon density of states is treated. Here, the atomic switching occurs more sharply and at a lower threshold than in model I. For the sake of simplicity and to establish proof of principle, we consider model I in what follows. A brief discussion of the influence of collective switching (model II) is given in Sec. V. Non-Markovian dynamics is not considered in the present paper.

When the atomic system is driven by a strong enough laser field, such that the dressed frequencies ω_{cw} , $\omega_{cw}-2\Omega_j$, and $\omega_{cw}+2\Omega_j$ are pushed away from the DOS discontinuity, the different spectral components of the Mollow triplet experience different densities of states and are described (model I) by different spontaneous emission decay rates $\gamma_0=2\pi\sum_\lambda g_\lambda^2\delta(\omega_\lambda-\omega_{cw})$, $\gamma_\pm=2\pi\sum_\lambda g_\lambda^2\delta(\omega_\lambda-\omega_{cw}\mp 2\Omega_j)$. Under this condition, the steady-state solutions of the dressed atomic operators (see Ref. [19] for details) are $\langle R_{12/21,j}(t)\rangle=\langle R_{12/21,j}(0)\rangle\exp(-\Gamma_{\text{coh},j}t)$, $\langle R_{3,j}(t)\rangle=[\langle R_{3,j}(0)\rangle-\langle R_{3,j}\rangle^{st}]\exp(-\Gamma_{\text{pop},j}t)+\langle R_{3,j}\rangle^{st}$. Here, $\Gamma_{\text{pop},j}=A_{+,j}+A_{-,j}$ is the decay rate for the atomic population, $\Gamma_{\text{coh},j}=\frac{4A_{0,j}+A_{+,j}+A_{-,j}}{2}$ is the decay rate for the atomic coherence, and $\langle R_{3,j}\rangle^{st}$ has the value $\langle R_{3,j}\rangle^{st}=\frac{A_{-,j}-A_{+,j}}{A_{-,j}+A_{+,j}}$, with $A_{0,j}=\gamma_0\mathbf{c}_j^2\mathbf{s}_j^2+\gamma_p\mathbf{c}_j^4\mathbf{s}_j^4$, $A_{-,j}=\gamma_-\mathbf{s}_j^4+4\gamma_p\mathbf{c}_j^2\mathbf{s}_j^2$, and $A_{+,j}=\gamma_+\mathbf{c}_j^4+4\gamma_p\mathbf{c}_j^2\mathbf{s}_j^2$. Here, a phenomenological parameter, γ_p , has been introduced describing the rate of atomic dipole dephasing due to interaction with phonons in the solid host. For $\Delta_{A,jL}>0$ and $\gamma_->\gamma_+$ as we consider here (see Fig. 7), the threshold cw laser field is

given by $A_j^{\text{cw}} = \frac{\hbar|\Delta_{Aj}| \sqrt{[4]\gamma_+\gamma_-}}{\mu \sqrt{[\gamma_+\gamma_-]}}$. At this threshold, the average value of the inversion operator changes sign and the QD switches from an absorptive state to an amplifying state on one Mollow sideband and from an amplifying to absorptive state on the other sideband.

After the nonlinear response of the QDs to the cw driving field has been established, the linear susceptibility of the j th QD to a weak probe beam is given (in the rotating wave approximation) by (see Ref. [19]),

$$\begin{aligned} \chi_j^{(1)}(\omega) &= \chi_{+,j}^{(1)}(\omega) + \chi_{-,j}^{(1)}(\omega) \\ &\sim \gamma_+ \mathbf{c}_j^4 (\pi_{2,j} - \pi_{1,j}) \frac{1}{[\omega - (\omega_{\text{cw}} + 2\Omega_j)] + i\Gamma_{\text{coh},j}} \\ &\quad + \gamma_- \mathbf{s}_j^4 (\pi_{1,j} - \pi_{2,j}) \frac{1}{[\omega - (\omega_{\text{cw}} - 2\Omega_j)] + i\Gamma_{\text{coh},j}}. \end{aligned} \quad (1)$$

In this formula, $\pi_{2,j} \equiv \langle R_{21,j} R_{12,j} \rangle_s \equiv \langle R_{22,j} \rangle_s = \frac{\gamma_- \mathbf{s}_j^4}{\gamma_- \mathbf{s}_j^4 + \gamma_+ \mathbf{c}_j^4}$ and $\pi_{1,j} \equiv \langle R_{12,j} R_{21,j} \rangle_s \equiv \langle R_{11,j} \rangle_s = \frac{\gamma_+ \mathbf{c}_j^4}{\gamma_- \mathbf{s}_j^4 + \gamma_+ \mathbf{c}_j^4}$ are the equilibrium excited and ground dressed state populations. In order to study light propagation through the photonic crystal waveguide with quantum dots resonantly driven by a high intensity cw laser beam, we sum the different susceptibilities of individual QDs $\{j\}$ using Eq. (1) and couple this total susceptibility to the optical field through Maxwell's equations. In what follows, we introduce a medium susceptibility defined in coordinate space $\vec{r} = (x, y)$ rather than the susceptibility (1) defined on individual atoms. The medium susceptibility is then allowed to vary randomly from point to point in the FDTD mesh (used to simulate electromagnetic wave propagation), in a manner consistent with the inhomogeneous distribution of QD transition frequencies. The proportionality constant, A [see Eq. (2)], is chosen such that for a given density of quantum dots, the overall medium susceptibility reduces to the conventional medium susceptibility [32,33] in the absence of the colored vacuum ($\gamma_+ = \gamma_-$) and in the absence of the cw driving field ($A^{\text{cw}} = 0$).

It should be noted that Eq. (1) contains the *nonlinear* response of the QDs to the cw driving field through the appearance of the Rabi frequency Ω_j . However, Eq. (1) describes only the *linear* response of the same QDs to a weak signal beam (the optical pulse that we wish to switch). In what follows, we extrapolate this linearized susceptibility expression into the region of moderate pulse amplitudes. A more detailed generalization to nonlinear pulse susceptibility will be presented elsewhere [31]. It is also important to point out that Eq. (1) is the *steady-state* susceptibility of QDs. In what follows, we apply this prescription to moderately short (picosecond scale) pulses. A more precise treatment of full time-dependent optical Bloch equations will be presented elsewhere [31].

The field dynamics is simulated numerically using the finite-difference time-domain method and the coupled nonlinear system of equations is solved. As a prerequisite to coupling the QD dynamics to the time-dependent Maxwell's equations, we convert the atomic susceptibility into the time

domain. For this purpose, we add the antiresonant (or counter-rotating) term [32], obtained by changing the sign of ω and then taking the complex conjugate of the resonant (rotating) term. This antiresonant term is usually neglected in the frequency domain but is needed to obtain a real susceptibility in the time domain. The inverse Fourier transform of the corrected susceptibility yields the real, time-dependent susceptibility,

$$\begin{aligned} \chi^{(1)}(x, y, t) &= 2 \text{Re}[\chi_+^{(1)}(x, y, t) + \chi_-^{(1)}(x, y, t)] \\ &= A e^{-\Gamma_{\text{coh}} t} [-\gamma_+ \mathbf{c}^4 (\pi_2 - \pi_1) \sin(\omega_{\text{cw}} + 2\Omega)t \\ &\quad - \gamma_- \mathbf{s}^4 (\pi_1 - \pi_2) \sin(\omega_{\text{cw}} - 2\Omega)t]. \end{aligned} \quad (2)$$

Here the parameters \mathbf{c} , \mathbf{s} , π_1 , π_2 , and Ω depend on $\vec{r} \equiv (x, y)$ according to the specific realization of QDs within the inhomogeneous distribution as described above. We assume that only one line of the elliptical rods, adjacent to the line of smallest rods, is seeded with quantum dots.

Our model for QD response is defined by fixing the proportionality constant A , such that susceptibility (2) reduces to the correct conventional linear susceptibility of a specified density of two-level dipole resonators in ordinary vacuum. In this situation, the frequency-dependent susceptibility is well known [33] and in the low-intensity regime is given by

$$\chi(\omega) = -\frac{\alpha_0(0)}{\omega_A/c} \frac{(\omega - \omega_A)T_2 - i}{1 + (\omega - \omega_A)T_2^2}, \quad (3)$$

where $\alpha_0(0) \approx \frac{|\mu|^2 T_2 N \omega_A}{\epsilon_0 \hbar}$, is the ordinary (linear) absorption coefficient at line center, ω_A is the line center transition frequency, μ is average dipole transition matrix element, T_2 is the dipole dephasing time scale (which for purely optical dephasing satisfies the relation $T_2 = 2T_1$, and N is the density of two-level systems. In order to compare (3) with (2) we set $\gamma_- = \gamma_+ = 1/T_1$ and $A^{\text{cw}} \approx 0$ ($\Omega = \frac{\Delta \omega}{2}$). Consequently: $\mathbf{s}^2 = 0$, $\mathbf{c}^2 = 1$, $\pi_1 = 1$, and $\pi_2 = 0$. Also $\Gamma_{\text{coh}} = \frac{1}{T_2} = \frac{1}{2T_1}$, for pure optical dephasing. Equation (2) then yields (in the rotating wave approximation)

$$\chi^{(1)}(\omega) = -A \frac{(\omega - \omega_A)T_2 - i}{(\omega - \omega_A)^2 T_2^2 + 1}. \quad (4)$$

By comparing Eq. (4) with Eq. (3), we identify

$$A = \frac{\alpha_0(0)}{\omega_A/c} \approx \frac{|\mu|^2 T_2 N}{\epsilon_0 \hbar}. \quad (5)$$

In what follows we interpret T_2 as the dephasing time, including the effect of phonons. As we will see in Sec. IV, the parameter, A , controls the switching contrast between absorption and gain. Our use of the steady-state susceptibility underestimates the actual switching contrast by assuming that the QD dipoles have equilibrated (dephased) with phonon degrees of freedom on time scales short compared to the optical field modulation. This is evident in Eq. (5) where a smaller value of T_2 implies a weaker QD response. In the crossover regime, when pulse duration and dephasing time scales are comparable, a stronger dipole response is possible [31].

In Eq. (2), the generalized Rabi frequency (as well as other parameters containing the Rabi frequency), is spatially dependent according to the light intensity distribution and the different transition frequencies of the QDs located in different positions inside the waveguide,

$$\Omega(x,y,t) = \left[\left(\frac{\mu A^{\text{cw}}(x,y,t)}{\hbar} \right)^2 + \frac{\Delta_{AL}^2(x,y)}{4} \right]^{1/2}. \quad (6)$$

Here, $A^{\text{cw}}(x,y,t) = \sqrt{2\langle [\mathbf{E}^{\text{cw}}(x,y,t)]^2 \rangle}$ is the amplitude of the cw laser field at the position (x,y) . The angular brackets denote a time-averaged electric field of the cw laser beam over a time interval long compared to the optical cycle, but short compared to other time scales of interest (signal pulse duration, response time of the medium, switching time of the device, etc.). In our numerical simulations, we perform a time average over three optical cycles.

We use experimental data [34,35] for InGaAs/GaAs and InAs/InGaAs as a guide for modeling our quantum dots. Accordingly we choose the QD dipole transition matrix element to have a magnitude

$$\mu = 1.09 \times 10^{-28} \text{ C} \cdot \text{m} \approx 12.857(ea_0),$$

where e is the electronic charge and a_0 is the Bohr radius (0.5 Å). The dephasing time of these quantum dots in the absence of an external driving field [36–40] is in order of nanoseconds at low temperatures. For illustration purposes, we choose the $T_2 = 4$ ns or equivalently $\gamma_p = 0.25 \times 10^9 \text{ s}^{-1}$. At room temperature, in the absence of an external driving field, the phonon-mediated dephasing time scale for a single quantum dot may be on the scale of a picosecond. In Sec. V of this paper, it is suggested that such rapid dephasing may be offset by collective response of a large number of QDs, experiencing a nearly identical driving field and thereby responding as a large collective dipole. Moreover, the application of a strong cw laser field on a single QD may directly impose coherence on the system [41] and thereby increase T_2 considerably from the experimental values quoted [36–40] in the absence of imposed coherence.

The choice of $T_2 = 4$ ns leads to suitable contrast between absorptive and amplifying states in our optical transistor for switching of optical pulses for the given QD density, dipole oscillator strength, and for a device (waveguide) length of about 10 microns. Ideally, all-optical switching should function at room temperature or higher. It is therefore important to experimentally test whether dephasing times can be prolonged by virtue of imposed coherence [41,42] from the cw laser driving field. Alternatively systems with larger dipole oscillator strengths, higher QD densities or weaker coupling to phonons must be considered. Collective switching effects (see Sec. V) may also play a vital role in sustaining high switching contrast at high temperature.

In a realistic 2D-3D PBG heterostructure, we expect that each pillar (of the defect line described above) contains on the order of 10 layers of QDs stacked on top of each other. Assuming that the average QD has a pyramidal shape with base 15 nm \times 15 nm and height 7 nm, that the lateral (x,y) spacing between QDs with one layer is 15 nm, and that there is 11 nm vertical spacing between QD layers, the QD density

is roughly $N = 6 \times 10^{16} \text{ cm}^{-3}$. In our idealized 2D model, we consider only a single layer of QDs. In order to account for more than one layer of QDs, it is necessary to map QDs from other layers into a single plane. As we describe later, this can be accomplished by using a finer FDTD mesh in our idealized 2D simulation and placing an artificial number (more than experimentally allowed packing density) on the single plane. In this mapping, the QD density parameter, N , is held fixed. However by including more QDs in the FDTD mesh, we obtain a better statistical representation of the inhomogeneous distribution. This also provides better numerical stability.

We choose realistic values [8] for the decay rates (above the waveguide cutoff in Fig. 4), $\gamma_+ = 10^9 \text{ s}^{-1}$, as for ordinary vacuum (free space). Below the waveguide cutoff, we assume [8] that the sudden onset of large density of electromagnetic modes leads to $\gamma_- = 100 \times 10^9 \text{ s}^{-1}$ for a 15-unit-cell-long nonlinear part of the waveguide. For a longer waveguide (24-unit-cell-long nonlinear waveguide) we choose [8] $\gamma_- = 500 \times 10^9 \text{ s}^{-1}$. In both cases we set $\gamma_0 = \gamma_+$, since the cw laser field oscillates above cutoff frequency (in order to prevent nonlinear coupling between the modes).

The precise evaluation of the spontaneous emission rates γ_+ (single-mode waveguide spectral region) and γ_- (bimodal waveguide spectral region) depends (according to Fermi's golden rule [43]) on the product of the dipole transition matrix element squared and the local electromagnetic density of states (LDOS) at the position of the quantum dots. First principles evaluation of these rates requires a 3D photonic crystal model where this LDOS is determined [8]. Moreover, the LDOS depends on the overlap of the electromagnetic mode amplitude with QD dipole. As a result γ_{\pm} may depend somewhat on the precise position of the QD within the waveguide architecture. We neglect these spatial variations in our model and simply choose fixed values of γ_+ and γ_- for given frequencies. Actual values of γ_+ and γ_- have been obtained through FDTD simulation of dipole oscillations in 2D-3D PBG heterostructures [8,44]. The decay rates are obtained directly by evaluating the flux of electromagnetic radiation through an imaginary closed surface surrounding the PBG waveguide architecture. The Purcell factor [22] is defined as the ratio of the total emission rate in the cavity to the emission rate from the same dipole oscillator in ordinary vacuum. Purcell factors of more than 2000 have been found [45] in the high LDOS region of the PBG waveguide (15 unit cells in length). Purcell factors in the single-mode spectral range of the same waveguide are close to 30. This strong radiative coupling to engineered modes in the PBG is an important factor in overcoming nonradiative relaxation and phonon dephasing effects. The large ratio of γ_-/γ_+ in our system arises from both the sudden cutoff of one of the waveguide modes as well as the difference in field overlap of the different waveguide modes with the QDs. Strong overlap of the fields with the QDs in the bimodal spectral region leads to radiative decay time scales on the order of a picosecond for one of the Mollow sidebands of the QD spectrum. In our calculations γ_{\pm} and γ_0 are chosen to be field independent parameters. In principle these spontaneous emission rates could also become dynamical variables in a system with strong nonlinearity in which the electromagnetic dispersion

relations and density of states are themselves altered by the presence of strong optical fields.

The detuning of the cw laser field from the QD line center is chosen to be $\Delta_{AL} = \omega_A - \omega_{cw} = 0.003(2\pi c/a)$, when the QD inhomogeneous broadening is 0.4% and is chosen to be $\Delta_{AL} = 0.0065(2\pi c/a)$ when the QD frequency distribution is 1%. The dynamical response of the QDs is then coupled to Maxwell's equations for the electromagnetic field in the waveguide. As a first illustration, we numerically solve Maxwell's equations (7a)–(7d) in the 2D PC waveguide Architecture 1 shown in Fig. 3, for TM polarized light by employing a piecewise linear recursive convolution approach [46,47]. The pulse and cw laser beams are well separated in frequency domain, so we use two sets of Maxwell's equations (with superscripts p and cw , respectively) in order to determine propagation characteristics of both beams,

$$\frac{\partial D_z^{p,cw}}{\partial t} = \left(\frac{\partial H_y^{p,cw}}{\partial x} - \frac{\partial H_x^{p,cw}}{\partial y} \right), \quad (7a)$$

$$\mu_0 \frac{\partial H_x^{p,cw}}{\partial t} = - \frac{\partial E_z^{p,cw}}{\partial y}, \quad (7b)$$

$$\mu_0 \frac{\partial H_y^{p,cw}}{\partial t} = \frac{\partial E_z^{p,cw}}{\partial x}, \quad (7c)$$

$$D_z^{p,cw}(x,y,t) = \epsilon_0 \epsilon_r(x,y) E_z^{p,cw}(x,y,t) + \epsilon_0 \int_0^t E_z^{p,cw}(x,y,t-\tau) \chi^{(1)} \times(x,y,\tau) d\tau. \quad (7d)$$

Here, μ_0 is the permeability of free space, ϵ_0 is the permittivity of free space, $\epsilon_r(x,y)$ is the dielectric constant of the undoped photonic crystal rods (for GaAs $\epsilon_r=9.0$), and $\chi^{(1)} \times(x,y,\tau)$ is the total susceptibility of the ensemble of QDs given by Eq. (2), within one line of elliptical rods with quantum dots. The total susceptibility has different values in each computational grid point in our FDTD simulation, determined by the different transition frequencies within our Gaussian distribution of quantum dots, randomly seeded in the active region, and according to the local cw laser intensity.

IV. NUMERICAL SIMULATION OF NONLINEAR WAVEGUIDE SWITCHING DEVICE

As a first set of numerical experiments, we launch an optical pulse at the input PC waveguide (from a source just adjacent to the absorbing boundary surrounding the computational domain) of spectral width covering relevant frequency range including both Mollow sidebands. The input power spectrum is denoted by $P_{in}(\omega)$. We consider two separate variations of waveguide Architecture 1 described in Fig. 3. In the first variation, the nonlinear part of this waveguide (Fig. 3) is 15 unit cells long. In the second variation, the active region is 18 unit cells long. We choose the lattice constant $a \approx 0.425 \mu\text{m}$ in order to investigate propagation of a pulse centered near $1.55 \mu\text{m}$ vacuum wavelength. Our

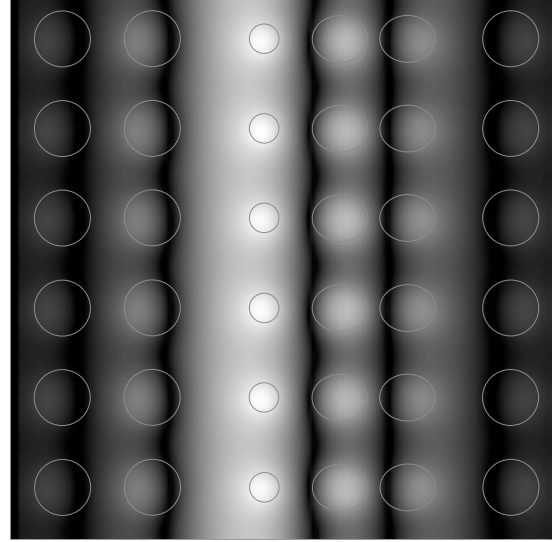


FIG. 8. Time-averaged electric field $\langle E(t) \rangle$ of the cw laser field propagating through mode 1 of the nonlinear waveguide shown in Fig. 3. In order to achieve maximal illumination of the quantum dots by the evanescent part of the field we seeded quantum dots only in the elliptical rods near the peak intensity of the propagating mode.

switching device is controlled with one external cw laser beam oscillating at frequency $0.278(2\pi c/a)$. For stable and efficient operation of the optical transistor, the illumination of the waveguide by this control beam should be stationary in time and have almost the same spatial distribution inside each nonlinear rod (see Fig. 8). We measure the spectral components of the transmitted pulse power, $P_{out}(\omega)$, using a detector placed at the output port of the waveguide (1 unit cell outside the nonlinear region). We define the spectrally resolved transmission coefficient as

$$T(\omega) = P_{out}(\omega)/P_{in}(\omega). \quad (8)$$

Our simulations demonstrate that it is possible to switch a 1 ps laser pulse from absorption to amplification and vice versa by a small change of the cw power (see Fig. 9). We find two spectral regions centered at $0.274455(2\pi c/a)$ and $0.28177(2\pi c/a)$ (corresponding to the Mollow sidebands of a QD with transition frequency at the center, ω_A , of the 0.4% inhomogeneously broadened distribution) where absorption, amplification, and switching occur. In order to estimate the actual threshold cw power needed for this specific device configuration, we map this 2D model system to a realistic 3D architecture [4,5,23] consisting of a $0.3a$ thick 2D microchip layer embedded in a 3D PBG material. This 2D microchip layer is assumed to be uniformly illuminated over its thickness in the third dimension and the light intensity is assumed to vanish abruptly at the 3D PBG cladding. This simplified picture provides a qualitative picture of the field pattern (that in reality is exponentially localized in the third dimension) in a 2D-3D PBG heterostructure waveguide. In this simple mapping, switching the pulse from absorption to amplification is easily achieved by changing the cw power from 1.35 mW to 2.8 mW. This relatively high intensity is required for

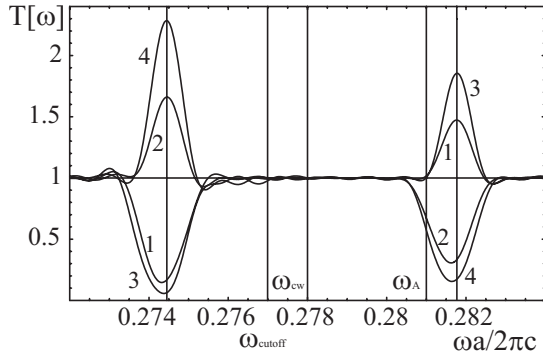


FIG. 9. Spectrally resolved power transmission of the signal pulse propagating through the nonlinear waveguide (Architecture 1) shown in Fig. 3, for two values (see below) of cw power oscillating at $0.278(2\pi c/a)$ in the standard mode of transistor operation. Amplifying maxima occur at Mollow sidebands [of 0.4% inhomogeneously distributed QDs around $\omega_A=0.281(2\pi c/a)$], located at $0.2744(2\pi c/a)$ and $0.2818(2\pi c/a)$. Lines 1 and 2 show switching of the transmission spectrum as cw power is changed in the 15-unit-cell-long nonlinear part of the waveguide seeded with 6×10^{16} dots/cm³. Lines 3 and 4 show transmission spectrum switching in the 18-unit-cell-long waveguide seeded with 8×10^{16} dots/cm³. If we assume that a realistic 3D waveguide consists of a $0.3a$ -thick 2D microchip layer sandwiched by 3D PBG materials, the cw power changes from 1.35 mW ($0.011 \text{ W}/\mu\text{m}$) to 2.8 mW ($0.022 \text{ W}/\mu\text{m}$) during the switching of the laser pulse spectrum.

Architecture 1 (Fig. 3), since the cw laser field (propagating in the linear dispersion mode) has only evanescent coupling to the QDs. Likewise this relatively large modulation of the control beam ensures that a significant fraction of QDs in the inhomogeneous distribution undergo switching from ground to excited state.

We observe that the overall contrast [ratio of maximum value of $T(\omega)$ to minimum value of $T(\omega)$ on a given Mollow sideband] increases with the number of QD layers in a given dielectric pillar and with the overall length of the active region. In the two variations of the present simulation, we effectively consider only two QD layers per dielectric rod. In variation 1 (waveguide seeded with 15 unit cells of QDs) we consider a QD density of $N \approx 6 \times 10^{16}$ dots/cm³ consisting of QDs placed on a square lattice, with lattice constant 30 nm, and vertically stacked with a spacing of 18 nm between layers. Numerically, we place individual QDs at each FDTD mesh point (with mesh spacing of 21 nm). This lateral FDTD mesh spacing is smaller than the physical spacing (30 nm) between QDs. In effect, our FDTD method imputes roughly double the number of QDs (1400) to a single layer than physically allowed. We interpret this as representing two layers of QDs in a 2D-3D PBG heterostructure. In variation 2 (waveguide seeded with 18 unit cells of QDs), our FDTD method likewise simulates two layers of QDs (1700 QDs in total within device). In variation 2, the QD volume density is chosen to be 8×10^{16} dots/cm³ (corresponding to a vertical separation between layers of 14 nm). Both variations 1 and 2 underestimate the total number of QDs that could participate in a real 3D switching device. For instance, in a real 2D-3D PBG heterostructure it may be possible to embed roughly 10

QDs layers in each of the active dielectric pillars, leading to considerably improved statistics of the QD distribution.

In our simulations, the peak amplitude of the electric field within the waveguide is about 10^5 V/cm , and about $6 \times 10^4 \text{ V/cm}$ inside the nonlinear elliptical rods. Such field strengths are well below the dielectric breakdown threshold in typical semiconductors. The required power levels for switching, scale inversely as the square of the QD dipole matrix element. For example, QDs with 2 times the transition dipole moment require only one-half the field magnitude and one-quarter the power level. This high field strength is made possible by the strong subwavelength focusing of the optical beam by the photonic crystal waveguide. This enables relatively large Mollow splitting (3% of QD central frequency) at relatively low overall power levels.

The device described above can operate in either of two modes. In the standard (preferred) mode of operation, the signal pulse is centered at a frequency close to the upper (high frequency) Mollow sideband of the QD distribution [$0.282(2\pi c/a)$]. In this case, a low power (1.35 mW) cw control beam leads to absorption (see Fig. 9 curves 2 and 4) of the signal [amplification occurs on the lower Mollow sideband at $0.274(2\pi c/a)$]. When the cw power is increased to 2.8 mW, the signal pulse centered at $0.282(2\pi c/a)$ is partially amplified (see Fig. 9 curves 1 and 3). This operation mode of the switch is advantageous since the signal pulse propagates through the single-mode spectral region of the waveguide. Consequently, there is little possibility of scattering or nonlinear coupling to the cutoff waveguide mode. In the reverse mode of operation, the signal pulse is spectrally centered near the lower Mollow sideband at $0.274(2\pi c/a)$. In the reverse mode, the lower power cw beam provides amplification (see Fig. 9 curves 2 and 4) and higher power cw field provides absorption (see Fig. 9 curves 1 and 3). The signal pulse now propagates in a spectral range where waveguide is bimodal. The reverse mode of operation is less stable because of the possibility of mode mixing.

The overall bandwidth of the absorption or amplification spectrum depends on both the QD size distribution and the spatial intensity variation of the optical fields that drive the quantum dots. In order to achieve overlap of the absorbing and amplifying fluorescence spectra, the bandwidth and the control field amplitude modulation must be chosen carefully. For a waveguide with a large jump in the photon density of states ($\gamma_- \gg \gamma_+$), operating near the threshold (for optical switching) driving field, the dressed frequency of a typical quantum-dot transition is $\omega_j \approx \omega_{cw} \pm 2\Omega_{th} \approx \omega_{cw} \pm \Delta_{AL} + \delta_j$, where δ_j is detuning (either positive or negative) of the j th quantum dot from the central atomic transition frequency ω_A . Therefore, the transmission spectrum bandwidth for a (hypothetical) uniformly illuminated QD ensemble operating near the threshold is equal to the QD transition bandwidth. For this hypothetical device to switch a 1 ps signal pulse, we require a QD distribution (bandwidth) $\{\delta_j\}$ of at least 0.2%. In the actual nonuniformly illuminated device, (near threshold) some fraction of QDs (with higher $\Delta_j = \Delta + \delta_j$ in the amplifying regime and with lower Δ_j in the absorbing regime) remain in the opposing state, reducing the transmission bandwidth. Our numerical simulations reveal that normally dis-

tributed quantum dots with FWHM of 0.4% provide the ideal broadening of the Mollow sideband spectrum that is both large enough to allow switching of a 1 ps signal pulse and that yields high contrast between absorption and amplification. Larger broadening enables faster switching, but the contrast between pulse absorption and amplification is diminished. This is a consequence of the decreased overlap of the absorption and amplification spectra as the system is modulated by a higher power gate field. Larger nonlinearity improves the switching effect.

In the reverse mode of device operation [signal pulse centered at $0.274(2\pi c/a)$], there is strong mixing of pulse energy between waveguide modes 1 and 2, leading to pulse reshaping. There is also an echo emitted after the main part of the pulse has been transmitted. This is a consequence of the cavity effect produced by the low group velocity mode.

In our idealized two-dimensional model (described by our FDTD mesh) we have considerably fewer quantum dots inside each nonlinear dielectric rod (around 90 dots per rod containing two layers of QDs) than is possible in a real 2D-3D PBG heterostructure (with 10 QD layers per rod). The distribution of the transition frequencies of the quantum dots differs for each rod leading to local random microcavities. As a result, for a small number of QDs, the transmission spectrum for the light propagating below cutoff frequency strongly depends on the specific realization of quantum dots. In further simulations (using QDs distributions with FWHM of 1%), we use a finer FDTD mesh (by increasing resolution to 30 pixels per lattice constant) and thereby double the number of QDs per rod. This represents close to four QD layers in a real 3D system. In this case, the signal transmission is less sensitive to the specific realization of QD placement within the device.

The time needed for a signal pulse to traverse the 15-unit-cell-long waveguide (variation 1) is approximately 0.1 ps. The group velocity of light in the single-mode waveguide is $0.2c$ where c is the speed of light in vacuum. If we assume that five additional unit cells on each side of the active region are required to connect this device with the rest of the PBG circuit, the total transit time for light of $1.55 \mu\text{m}$ vacuum wavelength through the microtransistor is still less than 0.2 ps. The switching time of the device is the time needed for the cw laser field to reconfigure and establish appropriate steady-state power and new nonlinear susceptibility inside the waveguide. Two signal pulses separated by more than the switching time (defined above) will experience distinct stationary responses of the nonlinear medium. Excessively rapid change of the cw power leads to spurious oscillations of the driving field inside the waveguide (see Fig. 10). These oscillations, in turn, produce temporal and spectral dispersion of a signal pulse passing through the microtransistor. In our numerical simulations we consider a driving field modulation in the form

$$E_z^{\text{cw}}(t) = \sin(\omega_{\text{cw}}t) \left\{ A_{\text{below}} + \frac{A_{\text{above}} - A_{\text{below}}}{2} \times \left[1 \pm \tanh\left(\frac{t - t_0}{t_{\text{switch}}/4}\right) \right] \right\}. \quad (9)$$

Here, A_{above} is the cw source amplitude needed for the work-

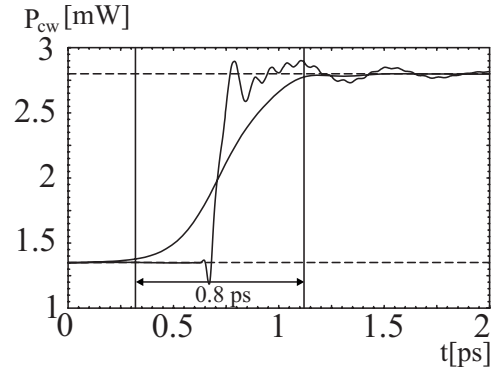


FIG. 10. Time-averaged power of the driving field measured at the transmission port of the nonlinear waveguide (Architecture 1), seeded with QDs inhomogeneously distributed around the central transition frequency $\omega_A=0.281(2\pi c/a)$, with FWHM of 0.4%. In the first curve (with irregular features) switching is implemented by instantaneous change of the source amplitude from the low to high cw power regime. In the smooth curve, switching is implemented more gradually [see Eq. (9)]. Units are rescaled for 2D-3D PBG heterostructure consisting of $0.3a$ -thick 2D layer sandwiched by 3D PBG materials.

ing regime above the switching threshold, A_{below} is the source amplitude needed for below threshold operation of the device, t_{switch} is the switching time, and t_0 is a parameter specifying the switching moment. We find that a change in gate power corresponding to $t_{\text{switch}}=0.8$ ps, eliminates spurious transients and we identify this as the practical switching time of the device. Our numerical studies demonstrate that the temporal profile of the signal pulse is preserved after amplification or absorption when the parameter t_{switch} is chosen appropriately and the standard mode of operation is employed.

For illustration and by way of contrast, we consider the reverse mode of operation and we launch two pulses, Gaussian in time, with temporal duration of 1 ps [56], separated in time by 5 ps, at the input port of the waveguide shown in Fig. 3. Using variation 1 of Architecture 1, we consider a driving field with $\omega_{\text{cw}}=0.278(2\pi c/a)$ whose power is switched (in reverse mode) from 2.8 mW to 1.35 mW (see Fig. 11). The nonlinear (15-unit-cell-long) part of the waveguide is seeded with $N=6 \times 10^{16}$ dots/cm³. We measure (see Fig. 11) the time-dependent power (averaged over one period of oscillation) of 1 ps laser pulses centered at frequency $0.274455(2\pi c/a)$ at the input and output ports of the waveguide, outside the nonlinear region. For reference, we also plot the driving field power at the entrance and exit ports of the device. We provide three FDTD data sets for each numerical experiment, corresponding to three different realizations of quantum dots selected from the overall Gaussian probability distribution. The magnitude of the absorption and amplification differs slightly from one realization of quantum dots to the next because of the small number of quantum dots used. When a larger number of QDs is used, self-averaging occurs with fewer realizations. We observe, most importantly, that the cavity effect of the waveguide cutoff mode together with the local random cavities, produced by a small number of quantum dots, leads to a noticeable echo after the

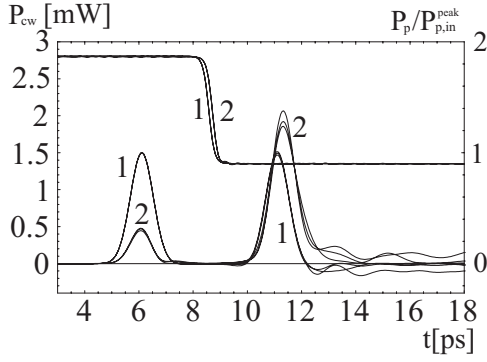


FIG. 11. Reverse mode operation of the optical transistor showing time-dependent power profile of the cw driving field (upper curves). Two consecutive laser pulses (lower curves), Gaussian in time, with temporal duration of 1 ps, centered at $0.274455(2\pi c/a)$, are measured at the input port (1) and output port (2) of the 15-unit-cell-long nonlinear part of the waveguide shown in Fig. 3. Here, $N=6 \times 10^{22}$ dots/m³ and the cw laser beam oscillates at $\omega_{cw}=0.278(2\pi c/a)$. Atomic transition frequencies ω_{A_j} are detuned from ω_{cw} and normally distributed around $\omega_A=0.281(2\pi c/a)$ with FWHM of 0.4%. Units of cw power are rescaled to represent a 2D-3D heterostructure consisting of 0.3a-thick 2D layer sandwiched by 3D PBG materials. Pulse power is measured in the units of peak power of the input pulse. Different curves at output port (2) correspond to different realizations of QDs.

main part of the signal pulse is transmitted (see Fig. 11). In order to avoid such noise in the optical chip, it is preferable for the device to operate in the standard mode at the frequency of $0.28177(2\pi c/a)$, where we have single-mode light propagation (see Fig. 12).

For illustration of the preferred operation of our microtransistor, we again launch two laser pulses with temporal duration of 1 ps, separated from each other by 5 ps, now oscillating at the central frequency of $0.28177(2\pi c/a)$ (standard mode of operation). These pulses propagate through the same waveguide and they are controlled with the same driving field power profile as in the case of reverse mode (com-

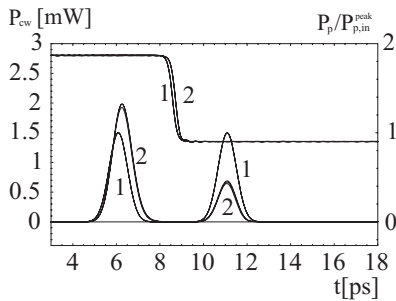


FIG. 12. Standard mode operation of optical transistor showing incident (1) and transmitted (2) time-dependent power of the cw driving field (upper curves) and two consecutive laser pulses (lower curves), Gaussian in time with temporal duration of 1 ps and central frequency of $0.28177(2\pi c/a)$, propagating through the 15-unit-cell-long nonlinear part of the waveguide shown in Fig. 3. All other parameters are the same as in Fig. 11. Here pulses propagate in the single-mode spectral region of waveguide and there is less noise at the output port (2).

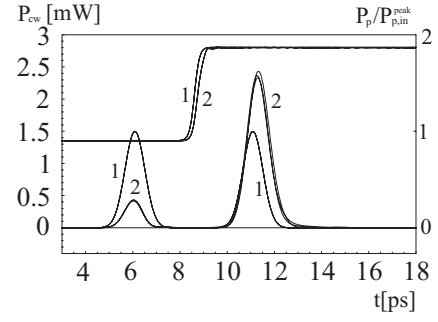


FIG. 13. Optical transistor in standard mode of operation showing temporal power profile of the cw driving field (upper curve) and two consecutive laser pulses (lower curves), Gaussian in time with temporal duration of 1 ps and central frequency of $0.28177(2\pi c/a)$, measured at the input (1) and output (2) end of the 18-unit-cell-long nonlinear part of the waveguide seeded with 8×10^{22} dots/m³. All other parameters are the same as in Fig. 11.

pare Figs. 11 and 12). However, there is now no light oscillating at the low group velocity mode (cutoff mode). We now observe no echo inside the waveguide after the pulse is transmitted (see Fig. 12). This is a significant advantage of the single-mode regime of the switching device (standard mode of operation) relative to the bimodal regime (reverse mode of operation). Furthermore, in the standard mode of operation, we observe much weaker dependence of the specific QDs realization. Variation 1 of our device amplifies the peak power of an input pulse to $P_{p,exit}^{peak}=1.37P_{p,in}^{peak}$ ($P_{p,in}^{peak}$ and $P_{p,exit}^{peak}$ are the peak power of the pulse measured at the entrance and exit port of the waveguide, respectively) and reduces peak power of the same pulse to $P_{p,exit}^{peak}=0.38P_{p,in}^{peak}$ in absorbing regime. For more ideal all-optical transistor action, we require higher amplification/absorption contrast. Accordingly, we discuss below, the efficacy of higher quantum-dot densities and longer effective nonlinear waveguides.

In Fig. 13 we present a signal pulse (in the standard mode of operation) propagating through (variation 2) the 18-unit-cell-long nonlinear part of the waveguide, seeded with $N=8 \times 10^{22}$ dots/m³. This enables amplification of the peak power of a 1 ps laser pulse centered at $0.28177(2\pi c/a)$ by more than 50% ($P_{p,exit}^{peak}=1.54P_{p,in}^{peak}$). Switching the cw power from 2.8 mW to 1.35 mW, reduces the peak power of the input pulse to $0.29P_{p,in}^{peak}$. Due to the nonuniform illumination profile of the nonlinear rods, some QD dipoles are always on the opposite side of the threshold and offset the overall amplifying or absorbing effect. Refinement of the device is possible through more careful placement of quantum dots, only in the small area of the peak illumination of elliptical rods (near small rods). Our numerical simulations show that such a reduction of the nonlinear area, in order to limit differential illumination (see inset in Fig. 14), can increase the amplification factor of the transmitted signal by an additional 15% and reduce maximal cw power by around 10%.

One way to reduce the holding power and gate power is to use a longer waveguide structure with larger jump of the electromagnetic density of states [8] near the waveguide cutoff frequency. We consider a PC waveguide with 24-unit-cell-long active region (variation 3 of Architecture 1) and 10-unit-cell-long ports on both sides (for smooth optical con-

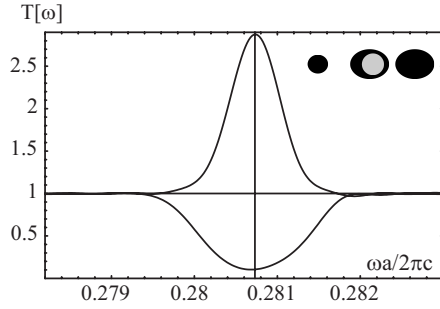


FIG. 14. Optical transistor transmission power spectrum in standard mode of operation for 24-unit-cell-long active region of the waveguide (variation 3 of Architecture 1) shown in Fig. 3, seeded with 6×10^{22} dots/m³, only in the small gray area (see inset), in order to eliminate cancellation from oppositely detuned quantum dots. For 2D-3D PBG heterostructure waveguide consisting of 0.3a-thick 2D layer sandwiched by 3D PBG materials, the cw driving power for amplification (upper curve) is 1090 μ W (0.0085 W/ μ m) and for absorption (lower curve) is reduced to 237 μ W (0.0019 W/ μ m). Driving field and central QD transition frequencies are located at 0.2775($2\pi c/a$) and 0.2805($2\pi c/a$), respectively, while amplifying maximum is at 0.280 73($2\pi c/a$). Here QD inhomogeneous broadening is 0.4%.

nection to the PBG circuit). This variation exhibits a 5 times larger jump of the local electromagnetic density of states [8] than variation 1. This reduces the required cw power in the waveguide by a factor of 2.5 and reduces the gate power to approximately 860 μ W. In Fig. 14, we present the optical power transmission spectrum for variation 3 of Architecture 1. Quantum dots are seeded only in the small gray area (see inset in Fig. 14), where the illumination pattern is more uniform. This reduces cancellation effects due to differentially driven quantum dots in opposing states. Further reduction of the cw driving power is possible using quantum dots with larger dipole moments. Quantum dots with 2 times larger dipole moments (achievable in certain semiconductor quantum dots [48–50] and colloidal quantum dots [51]) require only one-quarter the threshold intensity and gate power.

A key requirement for the operation of our all-optical switching device is the precision placement of a relatively narrow inhomogeneous distribution of QDs within a structured material. Recently developed experimental techniques based on lithographically defined nucleation sites [27–30], may enable highly ordered arrays of monodisperse quantum dots at prescribed positions inside a photonic crystal. A 1% size distribution of QDs is already experimentally feasible [52]. Accordingly, we describe the influence of this larger distribution of the transition frequencies on the efficiency of our microtransistor.

For a 1% relative distribution of QD transition frequencies, we increase the resolution of our FDTD simulation to 30 pixels per lattice constant in order to simulate a larger number of quantum dots. This serves to decrease the dependence of our results on specific quantum-dot realizations within the distribution. For a 1% distribution, we require higher powers in order to switch enough QDs into their excited state for overall switching of a signal pulse. Higher powers produce a nonlinear response of driving field itself.

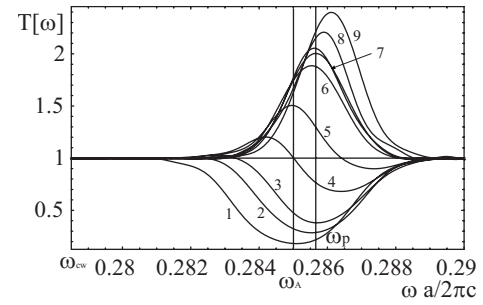


FIG. 15. Optical transistor power transmission spectrum for signal pulse propagating through 24-unit-cell-long nonlinear waveguide (variation 3 of Architecture 1) shown in Fig. 3, in standard mode of operation, for several values of cw powers: (1) 0.0 mW, (2) 1.4 mW, (3) 2.1 mW, (4) 3.6 mW, (5) 5.0 mW, (6) 6.6 mW, (7) 7.0 mW (for two different realizations of QD distribution; both curves are marked with an arrow), (8) 7.6 mW, (9) 8.5 mW, oscillating at 0.2785($2\pi c/a$). One line of elliptical rods (near the line of small rods), is seeded with 6×10^{22} dots/m³, normally distributed around central atomic transition frequency $\omega_A=0.285(2\pi c/a)$, with FWHM $\Delta\omega_A/\omega_A \approx 1\%$.

In order to reduce the refractive index change at the driving frequency, it is useful to further detune the driving field from the QD line center. This detuning leads to a higher switching threshold.

In Fig. 15, we show various transmission spectra of signal pulses propagating through the 24-unit-cell-long nonlinear part of the waveguide [variation 3 of Architecture 1 (see Fig. 3)], seeded with 6×10^{16} dots/cm³ normally distributed quantum dots with central atomic transition frequency $\omega_A = 0.285(2\pi c/a)$ and FWHM $\frac{\Delta\omega_A}{\omega_A} \approx 1\%$. The microtransistor is controlled by an external cw laser beam oscillating at $\omega_{cw}=0.2785(2\pi c/a)$ with power ranging from 0.0 to 8.5 mW. Here, the upper limit of the power range corresponds to 67 mW per micron of vertical (third dimension) thickness, Δz , of a waveguide in a 2D-3D PBG heterostructure with $\Delta z=0.3a$. With no driving field ($P_{cw}=0.0$ mW), all quantum dots are absorbing and the absorption spectrum is centered around ω_A with bandwidth given by the width of the quantum-dot distribution. Increasing the cw power (see curves 2 and 3 in Fig. 15), some quantum dots with lower threshold (with transition frequency closer to driving field frequency) and/or better illumination are switched to their amplifying state and the overall absorption of the signal is reduced at the lower end of the spectrum. Further increase of the cw power switches a larger number of QDs into the amplifying state, making the overall waveguide partly amplifying in the frequency range of the lower threshold quantum dots. However, the waveguide remains absorbing for higher frequencies (see lines 4 and 5). For large enough power ($P_{cw}=6.6$ mW), the majority of quantum dots become amplifying, and the absorption part of the transmission spectrum disappears. For a cw power of 7.0 mW, we have large amplification of the signal field inside the relevant, operating frequency interval. The operating frequency range is that which overlaps with the absorption spectrum in the low cw power working regime. We identify this power as most suitable for sustaining the optical transistor in the amplifying

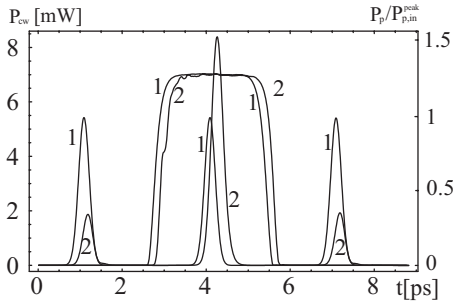


FIG. 16. Temporal power profile of the three consecutive 300 fs pulses (narrow peaks), Gaussian in time, separated from each other by 3 ps, measured at input port (1) and output port (2) of the 24-unit-cell-long nonlinear waveguide shown in Fig. 3. The cw driving field (broad central peaks) power is initially off, then turned on and, finally turned off and measured at input (1) and output (2) ports. Pulses are centered at $0.28565(2\pi c/a)$, while the cw laser field oscillates at $0.2785(2\pi c/a)$. One line of elliptical rods near the line of small rods, are seeded with 6×10^{22} dots/m³, normally distributed around central atomic transition frequency $\omega_A = 0.285(2\pi c/a)$, with FWHM $\Delta\omega_A/\omega_A \approx 1\%$.

regime. Further increase of the cw power (see curves 8 and 9), increases the amplification, but the amplifying spectrum shifts to higher frequencies. The reduced overlap with the absorbing spectrum makes this unsuitable for switching a signal pulse of a fixed frequency band.

In our all-optical transistor, the bandwidth of the transmission spectrum strongly depends on the bandwidth of the QDs transition frequencies. The device with 1% QD distribution can operate with shorter pulses and has shorter switching time than previously illustrated devices based on narrower QD distribution. The larger bandwidth device requires larger gate power. Nevertheless, the maximal intensity of the electric field in the amplifying regime of around 1.6×10^5 V/cm (10^5 V/cm inside nonlinear elliptical rods) remains well below dielectric breakdown threshold. In Fig. 16, we demonstrate switching of the 300 fs pulses, with cw power change from 0.0 mW to 7.0 mW and back to 0.0 mW. Our simulation yields a switching time of about one-half picosecond.

The performance of our optical switching mechanism depends crucially on the choice of PBG architecture. A better choice of structure can reduce power and increase amplification/absorption contrast. We demonstrate such an improvement using the structure (Architecture 2) presented in Fig. 5. In order to simplify the numerical simulations we use a slightly shorter nonlinear part of the waveguide (20 unit cells). However we retain the same waveguide parameters, γ_+ , γ_- , γ_0 , γ_p , same concentration of quantum dots, etc., as in Figs. 15 and 16. Since the dispersive properties of the waveguide in Architecture 2 differs from Architecture 1, we move the central transition frequency of the quantum-dot distribution above the waveguide cutoff frequency of Architecture 2. In particular, we choose $\omega_A = 0.3065(2\pi c/a)$ and keep the same FWHM of $\frac{\Delta\omega_A}{\omega_A} \approx 1\%$. The cw laser frequency in Architecture 2 is chosen to be $\omega_{cw} = 0.3(2\pi c/a)$ in order to keep the same detuning Δ_{AL} . Quantum dots are seeded in two outer lines of reduced rods where the highest jump

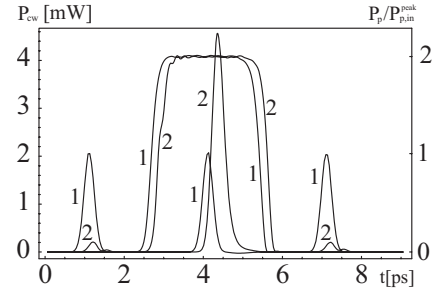


FIG. 17. Temporal power profile of the three consecutive 300 fs pulses, Gaussian in time, separated from each other for 3 ps, and cw laser beam, measured at input port (1) and output port (2) of the 20-unit-cell-long nonlinear waveguide shown in Fig. 5. The cw driving power (broad central peaks) is cycled through the off-on-off sequence and measured at both the input port (1) and output port (2). Pulses are centered at $0.30692(2\pi c/a)$, while the cw laser field oscillates at $0.3(2\pi c/a)$. Two outer lines of reduced rods are seeded with 6×10^{22} dots/m³, normally distributed around the central atomic transition frequency $\omega_A = 0.3065(2\pi c/a)$, with FWHM $\Delta\omega_A/\omega_A \approx 1\%$. Parameters of the waveguide are $\gamma_+ = \gamma_0 = 1 \times 10^9$ s⁻¹, $\gamma_-/\gamma_+ = 500$, and $\gamma_p = 0.5 \times 10^9$ s⁻¹, as in Figs. 15 and 16.

of the local electromagnetic density of states occurs. Our numerical calculations show that switching of the same three 300 fs pulses, as in Fig. 16, occurs with 40% lower power (compare Figs. 16 and 17). Despite the shorter nonlinear part of the waveguide, we obtain more than 6 times larger amplification/absorption ratios in Architecture 2 than in Architecture 1. This is due to better overlap of the propagating mode and nonlinear rods (QDs) in Fig. 5 than in Fig. 3. This result underscores the importance of further design optimization to improve the operating characteristics of the PBG all-optical microtransistor.

V. COLLECTIVE QD SWITCHING

In each of the simulations of all-optical switching, described above, it was assumed that individual quantum dots respond independently to the external laser fields. However, it is possible for collections of identical (or nearly identical) two-level systems responding to the same coherent electromagnetic field to act in unison as a large collective dipole resonator [6]. For identical atoms confined to a volume small compared to the cubic wavelength of their light emission, a deterrent to the observation of super-radiance [53] is the random dipole-dipole interaction (van der Waals dephasing) between the atoms. However if the Rabi frequency intensity of an external laser field is large [$\hbar\epsilon = \mu A^{cw} \approx (2-3)$ meV in our case] compared to the scale of dipole-dipole coupling (25μ eV in our case), the two-level systems may act collectively rather than independently. In a periodic dielectric microstructure (such as our PBG microtransistor) even QDs from different dielectric rods may respond collectively.

Collective resonance fluorescence consists of cooperative absorption and emission of radiation in the presence of external driving laser field. This offers important improvements in performance of our all-optical microtransistor. The steady-

state collective atomic response in a “colored vacuum” to strong laser fields has been solved previously [6,7,19]. Here, we briefly review some features of collective resonance fluorescence important for the present numerical investigation. Outside of the threshold regime, the sidebands of the scattered light spectrum are considerably broadened due to collective response. If $N_{\text{QD}} \gg 1$ quantum dots respond collectively, the sideband width becomes [19]

$$\Gamma_{\text{coh}}^{\text{coll}} = \Gamma_{\text{coh}} + N_{\text{QD}}(A_- - A_+) \left(\frac{2\langle n \rangle}{N_{\text{QD}}} - 1 \right). \quad (10)$$

Here, the average number of quantum dots in the excited dressed state is given by

$$\langle n \rangle = \frac{(N_{\text{QD}} + 1)A_-^{N_{\text{QD}}+1}}{A_-^{N_{\text{QD}}+1} - A_+^{N_{\text{QD}}+1}} - \frac{A_-}{A_- - A_+}, \quad (11)$$

where Γ_{coh} , A_{\pm} are defined in Sec. III.

It has been shown previously [19] that the frequency-dependant collective susceptibility of N_{QD} quantum dots is

$$\begin{aligned} \chi_{\text{coh}}^{(1)}(\omega) = & \frac{A}{2} \gamma_+ \mathbf{e}^4 (2\langle n \rangle - N_{\text{QD}}) \frac{1}{[\omega - (\omega_{\text{cw}} + 2\Omega)] + i\Gamma_{\text{coh}}^{\text{coll}}} \\ & + \frac{A}{2} \gamma_- \mathbf{s}^4 (N_{\text{QD}} - 2\langle n \rangle) \frac{1}{[\omega - (\omega_{\text{cw}} - 2\Omega)] + i\Gamma_{\text{coh}}^{\text{coll}}}, \end{aligned} \quad (12)$$

where the coefficient A is given by Eq. (5). If we replace $\Gamma_{\text{coh}}^{\text{coll}}$ with Γ_{coh} and set $N_{\text{QD}}=1$, Eq. (12) reduces to the susceptibility introduced in Sec. III. The collective scale factor, $N_{\text{QD}} - 2\langle n \rangle$, describes the enhanced response of a large number of QD dipoles acting coherently and in phase with each other. For example, if all QDs are initially in their ground state, then the collective response of N_{QD} dipoles $\mu_1, \mu_2, \dots, \mu_{N_{\text{QD}}}$ provides susceptibility proportional to $|\mu_{\text{coll}}|^2 \propto N_{\text{QD}}^2 \mu^2$, where $\mu_{\text{coll}} = \mu_1 + \mu_2 + \dots + \mu_{N_{\text{QD}}}$. However, the density of collective dipoles is reduced from the density of individual dipoles by a factor of N_{QD} . As a result, the susceptibility enhancement in collective response is a single multiplicative factor of N_{QD} .

We investigate the light propagation through the 13-unit-cells-long PC waveguide, presented in Fig. 5 (Architecture 2), seeded with quantum dots interacting collectively with an external driving field, using the numerical method described in Sec. V. Collective switching requires nearly uniform illumination of the quantum dots in question. More specifically, the energy scale of collective broadening of the fluorescence spectral features should exceed the energy scale of inhomogeneous broadening (arising from either QD size variations or local field amplitude variations). For a collection of 2000 QDs being pumped by an average electric field amplitude of 3.8×10^4 V/cm, the collective broadening energy scale is $\Gamma_{\text{coh}}^{\text{coll}} \approx 2.2$ meV.

In order to realize the conditions required for collective QD response, we place quantum dots only in a small area of the two outer defect lines of dielectric rods (see Fig. 18). More specifically, we choose a small circle with radius of $r=0.12a$, centered in the position of maximal illumination

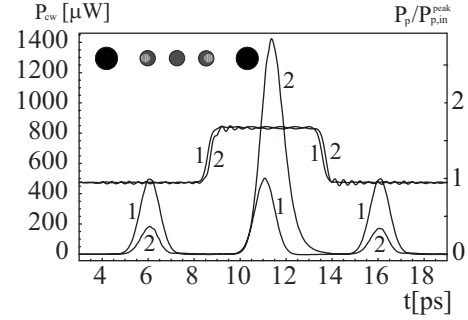


FIG. 18. Optical transistor action with collective QD switching. Curves depict temporal power profile of the cw driving field (broad central peaks) and three consecutive laser pulses (narrow peaks), Gaussian in time with temporal pulse duration of 1 ps each, and central frequency of $0.3024(2\pi c/a)$, measured ahead (1) and behind (2) the 13-unit-cell-long nonlinear part of the waveguide containing 2000 quantum dots responding collectively. Atomic transition frequency and driving field frequency are $0.302(2\pi c/a)$ and $0.2985(2\pi c/a)$, respectively. Units of cw power are adapted to describe waveguide in 2D-3D PBG heterostructure, while pulse power is measured in units of peak power of the input pulse. The gray area in the inset shows the position where quantum dots are located. Parameters of the waveguide are $\gamma_+ = \gamma_0 = 1 \times 10^9$ s⁻¹, $\gamma_-/\gamma_+ = 500$, and $T_2 = 2$ ps.

(see inset in Fig. 18). In the 13-unit-cell-long (variation 2 of Architecture 2) nonlinear part of the waveguide embedded in the 2D layer of a 2D-3D PBG heterostructure [24], approximately 2000 quantum dots may respond collectively. Our numerical simulations reveal that we can reduce or amplify the peak power of the 1 ps signal pulse by a factor of 2.7, using a cw power change (gate power) of around 350 μW. Here the magnitude of the electric field inside the nonlinear area remains below 4.0×10^4 V/cm ($I_{\text{max}} \approx 6.5$ MW/cm²). Further reduction of the switching intensity is limited by several factors. In our photonic crystal waveguides, the electromagnetic energy is not uniformly distributed but concentrated in the vicinity of dielectric rods. There is also significant intensity variation of light inside the dielectric rods. In the small area, shown in gray in the inset of Fig. 18, the magnitude of the electric field in the amplifying regime still varies by about 4×10^3 V/cm. For further reduction of the gate power, we require more uniform illumination of the nonlinear areas.

In general, a reduction in the number of QDs acting collectively, decreases the strength of the nonlinear response resulting in a weaker amplification to absorption contrast ratio. This can be offset by increasing the time scale of dipolar dephasing or choosing QDs with larger transition dipole matrix elements. However, when a smaller number of QDs is involved in the collective response, the collective broadening of the Mollow sidebands (away from switching threshold) is also reduced. This reduces the amplification and absorption bandwidth. In the absence of any inhomogeneous broadening, this leads to spurious tails (distortion) appearing in the transmitted pulses. A more realistic treatment of this problem requires a detailed understanding of the crossover between collective broadening and inhomogeneous broadening in the actual physical system.

Nevertheless, the possibility of collective QD response and collective switching in a periodic dielectric microstructure suggests that our microtransistor may function at room temperature where the dipole dephasing time for QDs may be on the order of 1 ps.

VI. DISCUSSION

In this paper we have demonstrated the remarkable and unique properties of photonic band-gap waveguide architectures in enabling subpicosecond switching of optical pulses using power levels at or below 1 milliwatt. This switching effect is based on Mollow fluorescence spectrum of quantum dots placed in a “colored” electromagnetic vacuum in which there is a large and abrupt jump in the local electromagnetic density of states as a function of frequency at the positions of carefully seeded QDs. While large Mollow splittings are difficult to achieve with low powers in conventional materials, the photonic crystal waveguide allows subwavelength focusing of light and the delivery of intense local fields at the locations of QDs. The photonic crystal waveguide also allows unprecedented engineering of the local electromagnetic density of states such that very strong coupling of light to QDs is possible over certain spectral ranges (leading to picosecond scale radiative lifetimes) but two or more orders of magnitude weaker coupling over an adjacent spectral range. Both spectral regions are characterized by significant Purcell factors. This engineered strong coupling is important for radiative effects to dominate dephasing and nonradiative relaxation effects from phonons.

We have demonstrated all-optical transistor action in PBG waveguides, seeded with quantum dots, and resonantly driven by one cw laser beam. Our numerical simulations confirm that less than 1 milliwatt modulation in power of the driving field can switch a 0.4%–1% inhomogeneously broadened distribution of QDs seeded within the PBG waveguide from the absorbing (most of the atoms are in ground state) to an amplifying state (most of the atoms are in excited state) for subpicosecond switching of signal pulses. This degree of QD inhomogeneous broadening is sufficient to prevent pulse reflection (due to impedance mismatch) and to provide bandwidth for amplifying pulses without incurring temporal distortion. The inhomogeneous broadening is also sufficiently

small to not require a trimodal waveguide architecture and LDOS filter construction as considered previously [8,19].

Our optical microtransistor device can be integrated in very high capacity optical networks operating at 200 Gbit/s. Operation powers of the device are in order of milliwatt, and maximal electric field magnitude in nonlinear area is below 6×10^4 V/cm. Improved architectures may enable even faster all-optical switching with higher capacity (more than 300 Gbit/s) operating with very short laser pulses with temporal duration of only 300 fs.

Finally, we presented a model with greater precision placement of QDs exhibiting collective response to the external driving field. In order for quantum dots to respond collectively it was necessary to reduce the nonlinear region to ensure nearly uniform illumination of all quantum dots. Smaller nonlinear area implies fewer quantum dots. Nevertheless, the collective QD system can switch 1 ps laser pulses and has a capacity of 200 Gbits/s. The gate power of this device is only 350 microwatt and switching time is below 1 ps. Most importantly, this collective switching effect survives dipole dephasing time scales close to 1 picosecond.

The outstanding challenges for experimental realization of our all-optical transistor are those of high precision material synthesis. Photonic crystal waveguides architectures must be made with a resolution of a few nanometers in order to achieve the required degree of electromagnetic density of states engineering [44]. Such high resolutions have already been achieved in 2D photonic crystal membrane structures [54,55]. This remains to be achieved in 3D PBG structures. The second challenge is the precision placement of nearly identical (<1% inhomogeneous broadening) quantum dots at specific locations within the PBG waveguide. If these challenges can be met, remarkable new all-optical functionality may be realized.

ACKNOWLEDGMENTS

The authors are grateful to Xun Ma, Dr. Rongzhou Wang, and Professor G. Bauer for some helpful discussions. This work was supported in part by the Natural Sciences and Engineering Research Council of Canada, the Canadian Institute for Advanced Research and the Ontario Premier’s Platinum Grant.

-
- [1] S. John, Phys. Rev. Lett. **58**, 2486 (1987).
 - [2] E. Yablonovitch, Phys. Rev. Lett. **58**, 2059 (1987).
 - [3] S. John, Phys. Rev. Lett. **53**, 2169 (1984).
 - [4] A. Chutinan and S. John, Phys. Rev. B **72**, 161316(R) (2005).
 - [5] A. Chutinan and S. John, Opt. Express **14**, 1266 (2006).
 - [6] S. John and T. Quang, Phys. Rev. Lett. **78**, 1888 (1997).
 - [7] S. John and M. Florescu, J. Opt. A, Pure Appl. Opt. **3**, S103 (2001).
 - [8] R. Wang and S. John, Phys. Rev. A **70**, 043805 (2004).
 - [9] M. F. Yanik, S. Fan, M. Soljagic, and J. D. Joannopoulos, Opt. Lett. **28**, 2506 (2003).
 - [10] H. Nakamura, Y. Sugimoto, K. Kanamoto, N. Ikeda, Y. Tanaka, Y. Nakamura, S. Ohkouchi, Y. Watanabe, K. Inoue, H. Ishikawa, and K. Asakawa, Opt. Express **12**, 6606 (2004).
 - [11] T. Tanabe, M. Natomi, S. Mitsugi, A. Shinya, and E. Kuramochi, Appl. Phys. Lett. **87**, 151112 (2005).
 - [12] G. W. Rieger, K. S. Virk, and J. F. Young, Appl. Phys. Lett. **84**, 900 (2004).
 - [13] M. Soljagic, E. Lidorikis, J. D. Joannopoulos, and L. V. Hau, Appl. Phys. Lett. **86**, 171101 (2005).
 - [14] J. H. Shapiro, Phys. Rev. A **73**, 062305 (2006).
 - [15] N. Moll, R. Harbers, R. F. Mahrt, and G.-L. Bona, Appl. Phys. Lett. **88**, 171104 (2006).
 - [16] D. Vujic and S. John, Phys. Rev. A **72**, 013807 (2005).

- [17] T. W. Mossberg and M. Lewenstein, *J. Opt. Soc. Am. B* **10**, 340 (1993).
- [18] M. Florescu and Sajeew John, *Phys. Rev. A* **64**, 033801 (2001).
- [19] M. Florescu and S. John, *Phys. Rev. A* **69**, 053810 (2004).
- [20] B. R. Mollow, *Phys. Rev. A* **5**, 2217 (1972).
- [21] D. P. Craig and T. Thirunamachandran, *Molecular Quantum Electrodynamics* (Academic, San Diego, 1984).
- [22] E. M. Purcell, H. C. Torrey, and R. V. Pound, *Phys. Rev.* **69**, 37 (1946).
- [23] A. Chutinan, S. John, and O. Toader, *Phys. Rev. Lett.* **90**, 123901 (2003).
- [24] A. Chutinan and S. John, *Phys. Rev. E* **71**, 026605 (2005).
- [25] K. Yee, *IEEE Trans. Antenn. Propag.* **14**, 302 (1966).
- [26] A. Taflov and S. C. Hagness, *Computational Electrodynamics*, 3rd ed. (Artech House, Boston, MA, 2005).
- [27] G. Bauer and F. Schäffler, *Phys. Status Solidi A* **203**, 3496 (2006).
- [28] G. Chen, H. Lichtenberger, G. Bauer, W. Jantsch, and F. Schäffler, *Phys. Rev. B* **74**, 035302 (2006).
- [29] Z. Zhong and G. Bauer, *Appl. Phys. Lett.* **84**, 1922 (2004).
- [30] Z. Zhong, O. G. Schmidt, and G. Bauer, *Appl. Phys. Lett.* **87**, 133111 (2005).
- [31] X. Ma and S. John (unpublished).
- [32] R. W. Boyd, *Nonlinear Optics*, 2nd ed. (Academic, San Diego, 2003).
- [33] R. L. Sutherland, *Handbook of Nonlinear Optics*, 2nd ed. (Dekker, New York, 2003), p. 357.
- [34] K. L. Silverman, R. P. Mirin, S. T. Cundiff, and A. G. Norman, *Appl. Phys. Lett.* **82**, 4552 (2003).
- [35] P. G. Eliseev, H. Li, A. Stintz, G. T. Liu, T. C. Newell, K. J. Malloy, and L. F. Lester, *Appl. Phys. Lett.* **77**, 262 (2000).
- [36] U. Hohenester, <http://physik.uni-graz.at/uxh/>
- [37] W. Langbein, P. Borri, U. Woggon, V. Stavarache, D. Reuter, and A. D. Wieck, *Phys. Rev. B* **70**, 033301 (2004).
- [38] P. Borri, W. Langbein, S. Schneider, U. Woggon, R. L. Sellin, D. Ouyang, and D. Bimberg, *Phys. Rev. Lett.* **87**, 157401 (2001).
- [39] M. Bayer and A. Forchel, *Phys. Rev. B* **65**, 041308(R) (2002).
- [40] A. S. Lenihan, M. V. Gurudev Dutt, D. G. Steel, S. Ghosh, and P. K. Bhattacharya, *Phys. Rev. Lett.* **88**, 223601 (2002).
- [41] Mesfin Woldeyohannes and Sajeew John, *Phys. Rev. A* **60**, 5046 (1999).
- [42] Tran Quang, M. Woldeyohannes, Sajeew John, and G. S. Agarwal, *Phys. Rev. Lett.* **79**, 5238 (1997).
- [43] Claude Cohen-Tannoudji, *Bernard Diu, and Franck Laloe, Quantum Mechanics* (Wiley, Toronto, 1997), Vol. II.
- [44] S. John and R. Wang, *Photonics Nanostruct. Fundam. Appl.* **2**, 137 (2004).
- [45] R. Wang (private communication).
- [46] A. Taflov and S. C. Hagness, *Computational Electrodynamics*, 2nd ed. (Artech House, Norwood, MA, 2000).
- [47] D. F. Kelley, *IEEE Trans. Antennas Propag.* **44**, 792 (1996).
- [48] J. R. Guest, T. H. Stievater, X. Li, J. Cheng, D. G. Steel, D. Gammon, D. S. Katzer, D. Park, C. Ell, A. Thränhardt, G. Khitrova, and H. M. Gibbs, *Phys. Rev. B* **65**, 241310(R) (2002).
- [49] S. Reitzenstein, A. Löffler, C. Hofmann, A. Kubanek, M. Kamp, J. R. Reithmaier, A. Forchel, V. D. Kulakovskii, L. V. Keldysh, I. V. Ponomarev, and T. L. Reinecke, *Opt. Lett.* **31**, 1738 (2006).
- [50] J. R. Reithmaier, G. Sek, A. Löffler, C. Hofmann, S. Kuhn, S. Reitzenstein, L. V. Keldysh, V. D. Kulakovskii, T. L. Reinecke, and A. Forchel, *Nature (London)* **432**, 197 (2004).
- [51] M. Shim and P. Guyot-Sionnest, *J. Chem. Phys.* **111**, 6955 (1999).
- [52] G. Bauer (private communication).
- [53] M. Gross and S. Haroche, *Phys. Rep.* **93**, 301 (1982).
- [54] T. Asano, B. S. Song, Y. Akahane, and S. Noda, *IEEE J. Sel. Top. Quantum Electron.* **12**, 1123 (2006).
- [55] S. Noda, *J. Lightwave Technol.* **24**, 4554 (2006).
- [56] We define the laser pulse duration as a time for which power of the pulse remains above 1/2 of its maximum.